Research Square

Preprints are preliminary reports that have not undergone peer review.
They should not be considered conclusive, used to inform clinical practice,
or referenced by the media as validated information.

Targeting the promoter RNA binding sites within Lassa virus L protein

Maria Rosenthal

rosenthal@bnitm.de

Bernhard Nocht Institute for Tropical Medicine https://orcid.org/0000-0003-2986-936X

Dominik Vogel

Bernhard Nocht Institute for Tropical Medicine

Gabriele Diana

Bernhard Nocht Institute for Tropical Medicine

Janna Scherf

Bernhard Nocht Institute for Tropical Medicine

Saskia Johanns

Bernhard Nocht Institute for Tropical Medicine

Jeanette Reinshagen

Fraunhofer ITMP https://orcid.org/0000-0002-8080-9170

Silke Olschewski-Pavlita

Bernhard Nocht Institute for Tropical Medicine

Claire Ortmann de Percin

BNITM https://orcid.org/0000-0002-2989-1463

Simon Rothbauer

Bernhard Nocht Institute for Tropical Medicine

Carola Busch

Bernhard Nocht Institute for Tropical Medicine

Morlin Milewski

Bernhard Nocht Institute for Tropical Medicine https://orcid.org/0000-0002-0164-4292

Markus Wolf

Fraunhofer Institute for Translational Medicine and Pharmacology (ITMP), Discovery Research ScreeningPort

Aaron Sweeney

Leibniz Institute of Virology (LIV) & Centre for Structural Systems Biology (CSSB)

Andrea Zaliani

Fraunhofer Institute for Translational Medicine and Pharmacology (ITMP), Discovery Research ScreeningPort

shgul123 Gul

Fraunhofer https://orcid.org/0000-0003-2543-1643

Maya Topf

Leibniz Institute for Virology (LIV), Universitätsklinikum Hamburg-Eppendorf UKE), Centre for Structural Systems Biology (CSSB) https://orcid.org/0000-0002-8185-1215

Philip Gribbon

Fraunhofer Institute for Translational Medicine and Pharmacology

---

Article

Keywords:

Posted Date: June 3rd, 2026

DOI: https://doi.org/10.21203/rs.3.rs-9528080/v1

License: This work is licensed under a Creative Commons Attribution 4.0 International License.
Read Full License

Additional Declarations: There is **NO** Competing Interest.

Targeting the promoter RNA binding sites within Lassa virus L protein

Dominik Vogel[1], Gabriele Diana[1,2], Janna Scherf[1], Saskia Johanns[1], Jeanette Reinshagen[3], Silke Olschewski-Pavlita[1], Claire Ortmann de Percin Northumberland[1], Simon Rothbauer[1], Carola Busch[1], Morlin Milewski[1], Markus Wolf[3], Aaron Sweeney[2], Andrea Zaliani[3], Sheraz Gul[3], Maya Topf[2,4], Philip Gribbon[3,*], Maria Rosenthal[1,3,4,*]

Affiliations

[1] Bernhard Nocht Institute for Tropical Medicine (BNITM), Research Group Structural Virology & Centre for Structural Systems Biology (CSSB), Hamburg, Germany
[2] Leibniz Institute of Virology (LIV) & Centre for Structural Systems Biology (CSSB), Hamburg, Germany
[3] Fraunhofer Institute for Translational Medicine and Pharmacology (ITMP), Discovery Research ScreeningPort Hamburg, Germany
[4] Institute for Molecular Virology and Tumorvirology, University Medical Center Hamburg-Eppendorf (UKE), Hamburg, Germany
* Co-corresponding authors

Abstract

The *Bunyaviricetes* class includes several human pathogens, such as the Lassa virus (LASV), which pose a significant threat to global health and impact the society and economy in affected countries of the Global South. At present, there are no antiviral treatments or vaccines approved to treat or prevent, for example, potentially fatal human Lassa fever. Relevant processes for the development of antiviral strategies include viral genome replication and transcription, which are catalysed by the multifunctional large (L) protein. Specific binding of the 3‘ and 5‘ viral genome termini to the L protein has been proven to be essential for these processes. Therefore, we investigated the tractability of the 3’ and 5’ RNA binding sites as drug targets. To this end, *in vitro* assays for high-throughput screening (HTS) of small molecule libraries were used to identify inhibitors of 3‘ and 5‘ RNA binding to the L protein. Two assays per binding site based on fluorescence polarization (FP) and homogenous time-resolved fluorescence resonance energy transfer (HTRF) were established and used for the orthogonal screening of a repurposing collection. Selected compounds were profiled in biochemical experiments and analysed for antiviral activity and cytotoxicity in cell-based assays. *In silico* analyses support the proposed mechanism of action of the hit molecule micafungin to inhibit 5’ RNA binding to L. We established the specific viral promoter RNA–polymerase interfaces as druggable targets and demonstrate the first pharmacological inhibition of a bunyaviral promoter RNA-binding site. This established early-stage drug discovery pipeline paves the way for the development of antiviral therapeutics against bunyaviruses and could also translate to influenza viruses.

Introduction

Lassa virus (LASV) is a member of the *Arenaviridae* family belonging to the order *Hareavirales* within the highly diverse class of *Bunyaviricetes* [1, 2]. As highlighted by the WHO's scientific framework for epidemic and pandemic research preparedness [3], LASV poses a significant threat to global health causing regular outbreaks of Lassa fever with potentially fatal outcome in West Africa [4, 5]. At present, no vaccines protecting from LASV infections or therapeutics for treatment of Lassa fever have been approved. As LASV is a biosafety level 4 pathogen, research towards the development of antiviral strategies is somewhat limited by the necessity for high-containment laboratories.

Antiviral drug discovery typically follows one of two strategies: a phenotypic approach, in which compounds are identified based on their ability to reduce viral replication in cell culture models without initially focusing on a specific molecular target, or a target-based approach, in which specific viral proteins are studied and compounds are evaluated using biochemical or binding assays to measure their functional effects on those defined targets [6]. Insights into the structure and function of LASV proteins have been increasing in the past years and offer potential avenues for target-based antiviral drug discovery. In particular, the L protein as a multifunctional viral protein with a central role in viral genome replication and transcription processes bears several functions that could be targeted: (i) the RNA-dependent RNA polymerase (RdRp) function resides within a highly conserved RdRp domain of the L protein and can likely be targeted by nucleoside analogues and non-nucleoside inhibitors. The (ii) cap-binding and (iii) endonuclease functions required for production of short capped RNA primers for viral transcription initiation, although structurally very similar to homologous domains of other bunyaviruses, have been shown to be inactive or weakly active *in vitro*, strongly limiting *in vitro* drug discovery approaches. In fact, for another bunyavirus family, the *Phenuiviridae*, despite clearly showing specific activity *in vitro*, the cap-binding site of the L protein has been found to have limited druggability [7]. For the endonuclease, several studies have been published on the development of targeted inhibitors, however, none of these have been clinically approved yet [8, 9]. (iv) The binding site of the viral 5' RNA terminus has been found to be essential for genome replication and transcription processes and activate the RdRp activity of L [10, 11]. (iv) Finally, the secondary binding site of the viral 3' RNA terminus, located

below the so-called pyramid domain, was also found to be essential for viral genome replication and transcription in cell-based mini-replicon experiments [10].

Targeting these viral RNA binding sites would theoretically also limit the potential for mutational escape of the virus from an inhibitor as this is an important virus-virus interface, which would require adjustment on both the protein and RNA sequences. However, so far it has not been attempted to target these sites.

Here, we developed high-throughput-feasible *in vitro* assays for screening of small molecule libraries against the 3' and 5' RNA binding sites of the LASV L protein. The screening strategy encompassed two orthogonal assays for each RNA binding site to reduce the number of false positive hits and use of a repurposing collection to validate assay performance and robustness. After hit confirmation in primary assays, validation experiments on compounds were performed *in vitro*, in cellular studies followed by mechanistic analysis based on *in silico* models.

This is the first established pipeline for high-throughput screening of small molecules interfering with viral RNA binding to the specific 3' and 5' RNA binding sites within the LASV L protein. This target-based approach demonstrates the significance of the specific viral RNA binding sites as targets for antiviral drug development against LASV and other bunyaviruses. It provides a solid foundation for broad screening campaigns and also opens opportunities for mechanism-of-action studies of inhibitors detected in phenotypic screening approaches.

Results

Target identification

Several studies on LASV and related Machupo virus (MACV) characterized the specific interaction of the highly conserved, untranslated 3' and 5' termini of each viral RNA segment (here denoted 3' RNA and 5' RNA) with the L protein [10-14]. Cryo-EM structures revealed distinct sites where the terminal 3' and 5' RNAs bind with the 5' RNA forming a characteristic hook-like conformation with an intramolecular base pair formed [10, 14]. 5' RNA binding leads to conformational rearrangements activating the L protein's RdRp activity [10, 14, 15]. During RNA synthesis elongation and in a presumed resting state of L, the terminal 7 nucleotides of the 3' RNA are bound to a 3' RNA secondary binding site of the L protein [10, 14, 16]. Biochemical studies are in line with this, revealing a maximum affinity of MACV L for the 7

terminal nucleotides of the 3’ RNA while longer RNA sequences did not show a significant additional increase [12]. For the 5’ RNA of MACV, biochemical studies demonstrated that a reduced length of 13 nt is enough to enhance RNA synthesis *in vitro* [15]. In LASV, the terminal 10 nt are enough to form the characteristic hook, including a non-templated G at the 5’ resulting from a prime-and-realign mechanism of genome synthesis initiation (therefore termed nt 0-9) [10, 11]. These biochemical studies all relied on electrophoretic mobility shift assays using radioactively labeled RNA oligonucleotides [11, 12]. This assay format, however, only has a low throughput, commonly requires additional components like unspecific RNA or BSA to optimize specificity and separation of the signals for bound and unbound fractions upon electrophoresis and is therefore not feasible for small molecule drug discovery at a reasonable scale. Additional evidence from cell-based studies emphasizes the biological significance of these specific RNA binding sites within L. Mutating residues in the 5’ RNA or 3’ RNA secondary binding site led to a total loss of function of viral genome replication and transcription in a mini-replicon system [10]. Therefore, targeting the 5’ and 3’ RNA binding sites with small molecules could inhibit viral genome replication and transcription.

Our goal was to establish high-throughput-compatible assay systems for detection and quantification of viral 3’ and 5’ RNA binding to the LASV L protein to enable small molecule screening campaigns. To reduce the number of false-positive hits from high-throughput screening (HTS), we employed two orthogonal assay principles: fluorescence polarization (FP) and homogeneous time-resolved fluorescence coupled to Förster resonance energy transfer (or homogeneous time-resolved fluorescence energy transfer, HTRF). We used purified LASV L protein (strain Bantou-289) [11] and designed short Cy5-labeled RNA oligonucleotides based on the structural data available [10].

Development and optimization of an FP-based HTS-feasible RNA binding assay

FP-based assays are well established for high-throughput applications [17, 18] and require labeling of one binding partner with a fluorophore, usually the smaller binding partner, which is called tracer. Polarized light is then used for excitation of only the fluorophores in a certain orientation causing fluorescence emission in a single plane. However, as molecules rotate in between excitation and emission, the emitted light is depolarized. Since the rate of rotation of molecules in solution is inversely proportional to their macromolecular size, binding of the

tracer to a protein, such as the L protein, results in a detectable reduction of depolarization. Consequently, if a small molecule affects this binding event, a change in the FP signal can be measured (Fig. 1A). Based on the structural data of L-RNA complexes [10] as well as biochemical data [10-12], tracers were designed consisting of the terminal 7 nucleotides (3' 1-7 nt) for the 3' RNA binding assay and consisting of the terminal 9 nt plus an extra G at the 5' end (5' 0-9 nt) for the 5' binding assay (Fig. 1B). These RNA sequences should retain the essential and specific interactions with the L protein and the 5' tracer should be able to form the observed hook-like 3D structure by intermolecular base pairing between nt 1 and nt 7, while being short enough to avoid additional movement independent of the L protein. For that same reason, short linkers between RNAs and the label were used (Supplementary Fig. 12). A Cyanine5 (Cy5) fluorophore label was chosen because it is well established in labeling of nucleic acids and its spectral properties in the red range of the electromagnetic spectrum reduce the probability of interference with small molecules in screening libraries, which often absorb or emit light with shorter wavelength (blue-violet) [17, 19]. To ensure the labels did not sterically hinder the interaction of the L protein with the 3' and 5' RNA, respectively, the Cy5 fluorophore was attached opposite the natural RNA terminus, i.e. at the 5' for the 3' RNA tracer and at the 3' for the 5' RNA tracer (Fig. 1B). Because small molecules binding to the 5' or 3' promoter binding sites remain to be discovered, conditions without L protein present were used as positive controls for maximum inhibition.

Tracer concentrations were set to 5 nM for the 3' RNA and 10 nM for the 5' RNA yielding sufficient fluorescence intensity signals for reliable assessment of the FP shifts. Tracer binding was characterized by titrating L protein against a constant concentration of tracer (Fig. 1C). From the resulting binding curves, Kd values were estimated to be around 6.1 nM (± 0.5 nM) for the 3' RNA and 83.8 nM (± 13.6 nM) for the 5' RNA. As a consequence, L protein concentrations of 10 nM and 50 nM were chosen to achieve an optimal assay window for the 3' and 5' RNA binding assay, respectively. Next, additional assay components were evaluated for their potential to enhance the assay window and stabilize the system, while still keeping the complexity of the assay at a minimum for HTS feasibility.

To reduce unspecific interactions of the RNA tracers with the protein and other material as well as L protein aggregation, we optimized the ion and detergent content in the reaction buffer as well as the assay plate material. We tested the influence of NaCl and KCl on the FP signal and found an optimum in a physiological range between 100-200 mM NaCl or KCl,

respectively (Supplementary Fig. S1A). Next, we evaluated the influence of Mg^{2+} and Mn^{2+} on the FP signal since these are known to be important for RNA folding [20], protein stability [21, 22] in general and for L protein function specifically [10, 23, 24] (Supplementary Fig. S1B). The 3' RNA binding assay was unaffected by the presence of Mg^{2+} ions (0.5-10 mM). At Mn^{2+} concentrations above 2 mM, a decrease in FP signal was observed. Similarly, the 5' RNA binding assay did not improve in the presence of increasing Mn^{2+} or Mg^{2+} concentrations but the signals were reduced. We did therefore not include Mn^{2+} or Mg^{2+} ions in the final assay. Addition of 0.1% (w:v) CHAPS in the buffer resulted in a lower FP signal of the unbound tracer likely due to reduced unspecific interaction of tracer and protein adsorption to the plate material (Fig. 1D). All assays were then adapted to automated screening conditions.

Development and optimization of an orthogonal HTRF-based HTS-assay

To reduce the number of false positive hits from HTS for validation in further experiments with significantly lower throughput, our strategy included development of an orthogonal assay. HTRF is a FRET assay that uses a monoclonal antibody coupled to a terbium (Tb) cryptate donor with a long fluorescence lifetime and a large Stokes shift (i.e., separation between the excitation and emission wavelengths). This Tb-cryptate antibody was used in combination with the same Cy5-labelled 3' and 5' RNAs from the FP assay as FRET acceptors. The long fluorescence lifetime of the Tb FRET donor helps eliminate short-lived background fluorescence (Fig. 2A). A Tb-cryptate labelled monoclonal anti-His tag antibody (Anti-6His mAb Tb-conjugate, Cisbio/revvity) was used as a FRET donor to bind to the C-terminal 6xHis tag at the LASV L protein. The assay components were optimized to achieve the lowest possible FRET acceptor concentration whilst maintaining a sufficient signal-to-background ratio. To this end, titrations were performed with the FRET acceptors 3'(1-7)-Cy5 or 5'(0-9)-Cy5, respectively, at constant concentrations of 75 nM L protein and 0.1 ng/µL Tb-cryptate mAb (as recommended by the manufacturer) (Fig. 2B). Under these conditions, at 10 nM of the 3'(1-7)-Cy5 and 30 nM of the 5'(0-9)-Cy5 tracer, respectively, signals were approximately double as high as the background. Reactions without L protein or an L protein with an internal StrepII-tag (L-StrepII) instead of a His-StrepII tandem tag (L-His) served as negative controls with no detectable difference between the two controls (Fig. 2B). Comparing mAb concentrations, both 0.1 ng/µl and 0.05 ng/µl mAb showed very similar performance (Supplementary Fig. S2).

Competition vs. displacement setup

Although the viral 3’ and 5’ RNA termini can bind to their specific pockets in the L protein outside of the RdRp active site, for a full cycle of genome replication both RNA termini need to be released at some point. Therefore, two biologically consistent assay setups were conceived: (i) a direct competition of small molecules and the tracer for the binding site and (ii) displacement of the tracer from the binding site by small molecules. As there were no established inhibitors available of 3’ or 5’ RNA binding to the L protein, both assay formats were evaluated for HTS-feasibility using the unlabeled viral RNAs as competitors. These experiments were conducted for both the FP and HTRF assays (Fig. 3).

To test the displacement setups, the respective 3’ and 5’ tracers were mixed with the L protein, and each mixture was incubated for 30 min to allow complexes to form. Unlabelled 3’ and 5’ RNAs (competitors), respectively, were subsequently titrated against the L protein-tracer complex. A non-specific, unlabelled polyA-RNA (9 nt) was used as a negative control. In the competition setup, the tracer was mixed with the competitor at different ratios and the L protein was added after 30 min. The equilibration time for stable measurements and an optimal assay window was 180 min (Supplementary Fig. S3). In the displacement assay setup, no significant concentration-dependent signal reversion to the baseline values could be observed for the HTRF and FP 3’ RNA binding assays, despite a 500-fold excess of competitor over the tracer (Fig. 3A and 3B, left panels; Supplementary Fig. S3). It appears, therefore, that the binding of the 3’ RNA to the secondary binding site of L is not easy to disrupt, not even by addition of the same amount of (unlabelled) RNA. This is likely due to the conformational changes in the pyramid region of L upon 3’ RNA binding [10]. For 5’ RNA binding, displacement of the labelled RNA in the HTRF assay was possible although not complete even at a 500-fold excess of the competitor. The resulting assay window was however sufficient for HTS (Fig. 3A and 3B, right panels). In the FP assay, the signals increased at competitor concentrations above 2 µM, suggesting nonspecific effects between the 5' tracer and the high RNA concentration in this assay setup (Supplementary Fig. S4). For this reason, the difference between the conditions with and without L protein (ΔFP) was analyzed here for both the 3’ and the 5’ RNA (Fig. 3B).

High-throughput screening against 3’ and 5’ RNA binding sites of LASV L protein

The final composition of the FP assay for HTS against the 3’ RNA binding site contained 12.5 nM of LASV L protein and 6 nM of Cy5-labelled 3’ RNA (nt 1-7) as a tracer in a final volume of 10 µl yielding a signal window (ΔFP) of about 200 mP. For the 5’ RNA binding site, the final FP assay contained 50 nM of LASV L protein and 10 nM Cy5-labelled 5’ RNA (nt 0-9) tracer in a final volume of 10 µl resulting in a signal window of about 100 mP.

The HTRF assay used a Tb-cryptate mAb concentration of 0.05 ng/µl in a final volume of 10 µl including 12.5 nM or 25 nM of L protein and 6 nM or 25 nM of 3’ RNA and 5’ RNA FRET acceptors, respectively. The signal window (ΔHTRF) was about 4000 counts for the 3’ RNA binding assay and about 3000 counts for the 5’ RNA binding assay.

For the 5’ RNA, both the FP and the HTRF assay were conducted in displacement format as it was considered more stringent in the selection of potent small molecules compared to the competition format. HTS against the 3’ RNA binding site was conducted using the competition format. In this setup the L protein was mixed with the small molecules first and then the tracer was directly added.

The Fraunhofer Repurposing Collection containing 5632 compounds [25] was used for screening at a constant compound concentration of 10 µM in 384-well plates using semi-automated dispensing of reagents and acoustic dispensing of small molecules. As a positive control (100% inhibition of RNA binding), conditions without L protein were used that contained either only the labeled RNA (FP) or additionally the FRET donor (HTRF). As negative controls (0% inhibition of binding), conditions without small molecules but with L and labeled RNA and with or without the FRET donor in case of the HTRF or FP assay were used, respectively. Z’ values above 0.5 demonstrated robustness and quality of the developed assays. Hit criteria are defined in the methods section. Screening results are summarized in Fig. 4 for the 3’ RNA and in Supplementary Figures S5 and S6 for the 5’ RNA assay.

Some 40 and 83 molecules were identified as primary hits in the 5' RNA screening using the FP assay in the two replicates n1 and n2, respectively, with 23 of these molecules identified in both replicates. Therefore, the total number of hit classified molecules from the FP-based 5’ RNA screening was 100. In the HTRF 5’ RNA screening, 25 and 75 molecules were classified as hits after 3 and 18 hours, respectively, with 21 of these overlapping. This resulted in a total of 79 primary hits from the HTRF-based 5’ RNA screening. Analysis of the overlap between

these two orthogonal assays (FP and HTRF) resulted in 23 molecules for further analysis. In addition, 9 molecules with inhibition values below 20% in the HTRF screening but values >20% in both replicates of the FP-based screening were also selected adding up to a total of 32 molecules for validation in dose-response experiments.

Based on the criteria specified for the 3'-RNA screening, a total of 204 compounds were classified as primary hits with 140 molecules identified only in the FP assay, 117 molecules only identified in the HTRF assay, and 53 classified as hits in both the FP and HTRF assays.

Hit confirmation and cell-based testing

The 204 hits of the 3' RNA screens were first retested at single concentrations in technical triplicates in both FP and HTRF assays and confirmed hits entered dose-response experiments (8-point titrations from 14 nM to 30 µM). All hits of the 5' screens were directly tested in dose-response experiments (10-point titrations from 2.5 nM to 50 µM) without intermediate confirmation. Selected dose response curves are presented in Fig. 5, additional curves are included in the supplement (Supplementary Fig. S7 and S8). Subsequently, compounds with an IC50 above 10 µM in both FP and HTRF assays were deprioritised. Compounds binding directly to RNA were removed by applying filters established by Kuzikov et al. [25], who previously performed a PicoGreen™ intercalation assay on the Fraunhofer Repurposing Collection. Only compounds with below 20% activity in the PicoGreen™ intercalation assay were retained. Additional consideration was given to the small molecule properties and bioactivity profiles [26] and thus compounds with reported high toxicity, potential for a covalent mechanism of inhibition, or without clear prospects for further development were removed. Finally, only compounds declared as hits in both orthogonal screening assays and those available for purchase at the respective time were taken forward. Applying all these selection criteria resulted in a total of 11 hits from the 5' and 3' RNA screening, each. Table 1 summarizes the performance of these hit molecules through all validation steps.

Selected compounds were then repurchased from commercial sources and re-tested in dose-response experiments, with 15 out of 22 hits reconfirming activity (Supplementary Fig. S9 and S10, Table 1). Subsequently, compounds were progressed to cell-based experiments. In preliminary studies, a viral mini-replicon system was employed, recapitulating viral genome replication and transcription processes under biosafety level 1 conditions [10, 27]. This system is commonly used with BSR-T7 cells, which are baby hamster kidney cells stably expressing

the T7 polymerase, and all additional components are co-transfected. The assay was scaled down from 24 to a 96 well format and titration studies showed addition of dimethyl sulfoxide (DMSO) up to 2% vol/vol was well tolerated. Ribavirin served as a positive control for the cell-based mini-replicon assay [27] (Fig. 6A). However, BSR-T7 cells were found to be sensitive to combined transfection and compound treatments, leading to unacceptably wide variability in measured cell viability and compound responses. Therefore, compounds were tested for their effect on LASV amplification on human A549 cells using complete viruses in a biosafety level 4 facility, with ribavirin and T705 (favipiravir) as positive controls. Both control compounds led to a reduction of viral titers with IC50 values of approximately 44 and 140 µM, respectively, with no apparent effect on cell viability (Fig. 6B). From all 17 tested compounds, micafungin was the only effective compound showing a reduction in LASV titers at a concentration of 200 µM whilst still non-toxic to cells (Fig. 6B), the IC50 was estimated to 195 µM. All other compounds tested, led to a severe decline in cell viability simultaneously as viral titers were reduced (Fig. 6B, Suppl. Fig. S11, Table 1).

Investigating the mechanism of action of micafungin

The screening assays were based on detecting the reduction of specific labelled RNA binding to L. To provide further evidence that the effect of micafungin was indeed specific, binding to L was tested using spectral shift analysis. This method measures changes in the chemical environment of a dye covalently linked to the L protein upon binding of a small molecule. Micafungin was indeed found to cause a concentration-dependent spectral shift, strongly indicating direct binding to the L protein (Fig. 7A). As binding of the 5’ RNA had been shown to boost polymerase activity of L, an impairment of 5’ RNA binding to L in presence of an inhibitor may influence *in vitro* polymerase activity. Therefore, primed *in vitro* RNA synthesis in the presence of micafungin was tested (Fig. 7B). The relative effect of micafungin on primed RNA synthesis by the L protein seems independent of the presence of the 5’ RNA. However, in absolute terms, the boosted signals were reduced to background levels in the same concentration range and with a very comparable IC50, which is also very close to the Kd determined in the screening assay. Therefore, micafungin might simultaneously affect both the RNA synthesis activity and the boosting effect by the 5’ RNA or the RNA synthesis alone.

In silico analysis of micafungin’s potential to bind to the 5’ RNA binding site of L

To investigate whether micafungin could bind to LASV L protein and identify possible micafungin binding modes, a computational workflow was employed, which integrated consensus binding site identification with precision docking (Suppementary Fig. S13, see methods). Three consensus sites were identified by both AF3 [28] and AutoDock Vina [29] using a model of the full-length L-protein. One of these sites was within the 5’ binding site and subsequently selected for further refinement.

Precision docking on this site was performed on the experimentally resolved structure (7OJN) of the protein using a consensus docking approach (Supplementary Fig. S13, see methods) [30]. This structure was chosen because it represents the RNA-bound state, in which the sidechains better reflect the bound environment. Docking of the full ligand did not produce a strict consensus between the two methods, likely reflecting the large size and high conformational flexibility of micafungin (31 rotatable bonds, Fig. 7C). However, two of the full ligands poses agreed in the positioning of the sulphate moiety within a positively charged cavity of the binding site, while the macrocycle adopted a very similar conformation. In contrast, the orientation of the aromatic tail was not consistent (Fig. 7C). To better sample this region, the aromatic tail fragment was docked separately, generating a consensus orientation within a cleft of the binding site. Notably, this consensus overlapped with the attachment point of the macrocycle in one of the full ligand poses. Based on the agreement of the sulphate hotspot, the macrocycle conformation and the consensus aromatic tail orientation, this pose was selected for further refinement (Fig. 7D).

In our models, micafungin stretches along the left side of the 5’ RNA binding site, overlapping with the region accommodating the first four nucleotides of the RNA (Supplementary Fig. S14). This binding mode involves several polar and non-polar interactions. In particular, the sulphate moiety forms electrostatic and hydrogen bond interactions with positively charged residues that normally coordinate with the RNA phosphate backbone. Additional hydrogen bonds and hydrophobic contacts are formed along the aromatic tail, which inserts into a cleft normally occupied by the first guanine (G0). The aromatic tail while the macrocycle extends along the pocket. These interactions are consistent with the observed competition between micafungin and the 5’ RNA, supporting the hypothesis that micafungin may bind to the 5’ RNA binding site of LASV L. However, it cannot be excluded that the compound binds to alternate sites within the L protein. Nevertheless, the concordance of biochemical, biophysical and virus

amplification inhibition effects supports the use of our screening approach to target the interface of LASV L protein and the viral RNA.

Discussion

The general antiviral strategy explored here to target the specific RNA-binding sites within the viral L protein presents several benefits: The genomic RNA termini are essential for specific recognition of the viral RNA template by the viral polymerase (i.e., the L protein). When this recognition is impaired, the L protein would likely also associate non-specifically with other RNAs of the cell, limiting efficiency of both viral genome replication and transcription processes and potentially changing the localization and composition of viral replication foci within the cell. An evasion of this inhibition by selection of resistant virus mutants is, however, unlikely as mutations of the RNA binding site would most likely have to be accompanied by mutations in the viral genome termini. The likelihood of an emergence of a viable combination of such mutations can be considered extremely low. The development of multiple inhibitors targeting distinct essential functions within a virus life cycle for a combination therapy has been established, for example, as a standard therapy for human immunodeficiency virus (HIV) and hepatitis C virus (HCV), which also mutate at high frequency [31-34]. The biochemical stage hits derived from our screening approach did show a minimal overlap (3 compounds, Saroglitazar, Salirasib and GW-3965) between the 3' and the 5' RNA binding sites, which leaves the possibility of a common pocket for allosteric regulation of viral RNA binding to L. Overall, the hit rates were generally normal for HTS involving bioactive compounds with values between 1.4 and 3.6%. The use of repurposing collections for HTS can significantly reduce the time, cost, and risks associated with drug discovery as many of the molecules are well characterized in terms of ADMET (Absorption, Distribution, Metabolism, Excretion, Toxicity), pharmacokinetic and pharmacodynamic properties as well as, in some cases, clinical safety data [25, 26, 35]. In this study, however, many of the hit molecules were found to cause cytotoxic effects in the cell lines used for the mini-replicon experiments and the virus growth inhibition studies. This was not foreseeable and limited the scope of cell-based experiments. For micafungin, the availability of the compound in the cell could be a problem. It has been predicted to have poor oral bioavailability [36], is therefore applied intravenously to patients, and was shown to be highly protein bound in the blood plasma (99.8%). While red blood cells do not significantly take up micafungin, intracellular concentrations in peripheral white blood

cells and lung cells were found to be approximately 10-fold and 5-fold higher, respectively, than corresponding plasma concentrations [36, 37]. However, although a lung cancer cell line (A459) was used for the viral growth inhibition experiments, intracellular availability of micafungin was not confirmed. Therefore, it is still possible that (i) micafungin might not have entered the cells efficiently, (ii) the compounds preferred location in the cell might be different from viral genome replication and transcription processes (potentially phase-separated, membrane-less organelles), (iii) the compound may be metabolized at a high rate inside these cells, or (iv) the compound may be actively removed from the cell cytoplasm by an efflux pump such as the p-Glycoprotein [38]. Micafungin is known to be metabolized by arylsulfatase, catechol-*O*-methyltransferase, and several cytochrome P450 (CYP) isoenzymes (3A4, 1A2, 2B6 and 2C) [36]. However, at least for the catechol-*O*-methyltransferase a lower activity in A549 cells compared to hepatic and kidney cells has been demonstrated [39] and the CYP profiles do not indicate an induction of the relevant isoforms in A549 cells [40]. We also tested a combination treatment of LASV infected A549 cells with the p-Glycoprotein inhibitor CP-100356 and micafungin (Supplementary Fig. S15). Inhibition of p-Glycoprotein has been used successfully in combination with a protease inhibitor against SARS-CoV-2, resulting in the combination therapeutic known as Paxlovid [41, 42]. However, no change in the effect of micafungin on LASV replication has been observed. In summary, it is unclear why micafungin only presented an antiviral effect on LASV at rather high concentrations in A549 cells. Due to the compounds' properties and also administration preferences, it does not represent a promising molecule for further drug development steps. However, the observed effect in cell culture and the additional in vitro and in silico data presented in this work support the conclusion that the specific RNA:protein interfaces of bunyaviruses are druggable.

Despite the high sequence diversity in bunyaviruses, the hook-like structure of the 5' RNA termini bound by the respective L proteins is very similar [24]. Even in influenza viruses, the 5' RNA termini are bound to the polymerase complex in a very similar manner. In addition, all bunyaviruses and influenza viruses also harbor specific binding pockets for the 3' RNA termini in their polymerase proteins. Therefore, these protein:RNA interfaces may represent virus-specific targets with broad relevance for segmented negative-strand RNA viruses.

The 3D RNA structures of the 5' genome termini themselves might also represent druggable targets [43] that could be explored using the presented pipeline and respective small molecule collections binding to RNA.

The established screening assays and the orthogonal screening approach presented here have been demonstrated to be highly robust and selective. They require a standard screening infrastructure and allow for high-throughput target based screening against highly pathogenic viruses at a low biosafety level. High-safety lab infrastructure is only required for validation steps. The screening assay principles can be also used for mechanism of action studies of compounds resulting from phenotypical antiviral screening. Transfer of the assay principles to assess L protein:RNA interactions in other bunyaviruses will enable selection of potentially broad-acting molecules. In summary, we here presented a target-based high-throughput early drug discovery pipeline against LASV validating the specific viral RNA binding sites of the L protein as promising targets for antiviral therapies.

Methods

Expression and purification of LASV L protein

The L gene of LASV Bantou 289 (GenBank accession no. MK044799) containing a His-StrepII tandem tag at the C terminus (L-His) was used for baculovirus production and protein expression in Hi5 insect cells as described previously [11]. Harvested insect cells were resuspended in 50 mM HEPES(NaOH) pH 7.0, 1 M NaCl, 10% (w/v) glycerol and 2 mM dithiothreitol, 0.05% (v/v) Tween20 and protease inhibitors (Roche, cOmplete mini), lysed by sonication and centrifuged two times (20,000 × *g* for 30 min at 4 °C). Strep-TactinXT beads (IBA) were used for affinity purification and the protein was eluted with 50 mM Biotin (Applichem) in 50 mM HEPES(NaOH) pH 7.0, 500 mM NaCl, 10% (w/v) glycerol and 2 mM dithiothreitol. L protein-containing fractions were pooled and diluted 1:1 with 20 mM HEPES(NaOH), pH 7.0 before heparin chromatography (HiTrap Heparin HP, GE Healthcare) and one-step elution in 50 mM HEPES(NaOH), pH 7.0, 1 M NaCl, 10% (w/v) glycerol and 2 mM dithiothreitol. The protein was concentrated using centrifugal filter units (Amicon Ultra, 30 kDa MWCO), flash frozen and stored at −80 °C. Protein integrity was checked by SDS-PAGE and an A260/A280 ratio (as an indicator for contamination by nucleic acids) of 0.6 was considered acceptable.

Fluorescence polarization binding assay

LASV L protein was used either in combination with Cy5-labeled 3’ (nt 1-7, 3’-HO-GCGUGUC-(linker)-Cy5-5’) or 5’ (nt 0-9, 5’-Cy5-(linker)-GCGCACCGGG-OH-3’) RNA termini of the L

segment as a tracer. Linker structures are presented in Supplementary Fig. S12. For HTS, this assay was performed either in competition (3') or displacement (5') format in 10 mM HEPES(NaOH), pH 7.0, 200 mM NaCl, 0.1% CHAPS (w/v). Positive and negative assay controls contained the tracer only or tracer and L protein, respectively, as well as 0.1% DMSO. Compounds to be screened were stored at -20°C in 100% DMSO and transferred by acoustic dispensing (Echo 550R, Labcyte Inc./Beckmann Coulter) to the assay plates (Greiner Small Volume 384-well Black Flat Bottom Polystyrene Non-Binding Microplate, Prod. Nr 784900). In competition format, L protein was added first followed by a 30 min incubation period at room temperature, before addition of the 3' RNA tracer. In displacement format, tracer and protein were pre-incubated for 30 min at room temperature mixing with the compounds in the assay plates. Plates were sealed with tin foil during incubation time. After 2 h incubation at room temperature FP signals were measured using an Multilabel Reader (2103 EnVision™ HTS Microplate Imager, PerkinElmer, USA) with an excitation wavelength of 620 nm (filter X620, BW=40 nm), and emission recording at a wavelength of 688 nm via the P channel (filter M688p, BW=45 nm) and the S channel (filter M688s, BW=45 nm).

The final concentrations of specific assay components were 50 nM LASV L, 10 nM 5'(nt 0-9)-Cy5, 10 µM compound and 0.1% DMSO in a total volume of 10 µL/well for the displacement format; and 12.5 nM LASV L, 6 nM 3'(nt 1-7)-Cy5, 10 µM compound and 0.1% DMSO in a total volume of 10 µL/well for the competition format.

Homogenous time resolved FRET assay

LASV L protein was combined with an anti-6HIS Tb cryptate gold-labelled mAb (Cisbio) as FRET donor and either the Cy5-labeled 3' (nt 1-7) or 5' (nt 0-9) RNA of the L segment as FRET acceptors, respectively. The assay was performed either in competition (3') or displacement (5') format in 10 mM HEPES(NaOH), pH 7.0, 200 mM NaCl, 0.1% CHAPS (w/v). Positive and negative controls contained the FRET acceptor (Cy5) and donor (Tb cryptate) in absence or presence of the L protein, respectively, as well as 0.1% DMSO. Compounds to be screened were stored at -20°C in 100% DMSO and transferred by acoustic dispensing (Echo 550R, Labcyte Inc./Beckmann Coulter) to the assay plates (Corning® Low Volume 384-well White Flat Bottom Polystyrene NBS Microplate, Prod. Nr 3824). Initially, L/donor complex formation was performed by mixing the antibody coupled to the FRET donor with the L protein in the

assay buffer and incubation for 15 min at room temperature. In displacement format, this complex was then incubated with the 5' FRET acceptor oligo (Cy5) for 30 min at room temperature before it was added to the assay plate containing the compounds. In competition format, the L/donor complex was added first to the assay plate containing the compounds and the 3' FRET acceptor oligo (Cy5) was added after a 30 min incubation period at room temperature. HTRF signals were measured after 3 h and/or 18 h incubation at room temperature using an Multilabel Reader (2103 EnVision™ HTS Microplate Imager, PerkinElmer/Revvity) with an excitation wavelength of 340 nm (filter X340, BW=60 nm) and emission detection at wavelengths of 665 nm (filter M665, BW=75 nm) and 620 nm (filter X620, BW=10 nm) after a time delay of 120 ms.

Hit criteria, filtering and statistical analysis

Assay robustness of the FP and HTRF assay was assessed via the Z' value and only experiments resulting in a Z' > 0.5 were considered [44]. Hit criteria for FP-based 5' RNA HTS were: (i) Inhibition (%) > Inhibition (mean negative) (%) + 4σ (meaning an inhibition of more than 20% in this case); (ii) optical interference I(S) had to fulfill the criterion of $I_{neg}(S)(mean) - 3\sigma < I(S) < I_{neg}(S)(mean) + 3\sigma$; (iii) hit criteria had to be met in either replicate n1 or n2. Hit criteria for HTRF-based 5' RNA HTS were: (i) Inhibition (%) > Inhibition (mean negative) (%) + 4σ (meaning an inhibition of more than 20% in this case); (ii) I(Donor) should be within ± 5σ of a linear regression between the positive and negative controls in the assay; (iii) hit criteria had to be met in either the readout after 3 h or 18 h. Except for (iii), the same criteria applied for the HTRF-based 3' HTS. For the FP-based 3' HTS criterion (ii) was set to $I_{neg}(S)(mean) - 5\sigma < I(S) < I_{neg}(S)(mean) + 5\sigma$, and there were no biological replicates to consider.

At the intermediate confirmation step (single concentration retesting) of 3' RNA hits, compounds that did not confirm the inhibition rates from the screening or showed less than 20% inhibition in either the FP or HTRF assays were excluded. Plotting and fitting of dose-response data was performed with GraphPad Prism version 10.6.0. The models used for curve fitting are indicated in the respective figure captions.

LASV mini-replicon system

The experiments were performed in the context of the T7 RNA polymerase-based LASV (strain Bantou 289) mini-replicon system [11, 27]. In a 96 well plate 1.1 x 10^4 BSR-T7/5 cells/well

stably expressing T7 RNA polymerase [45] were seeded. After 24 h, cells were transfected per well with 50 ng of pCITE2a-minigenome plasmid expressing renilla luciferase (Ren-Luc), 50 ng of pCITE2a-L expressing either LASV L protein wildtype or a catalytically inactive mutant, 50 ng of pCITE-NP expressing NP, and 10 ng of pCITE-FF-Luc expressing firefly luciferase as an internal transfection control using Lipofectamine 2000 according to the manufacturer's instructions. At 4h after transfection, the transfection mix was replaced by 100 µL/well GMEM (Gibco) supplemented with 5% FCS and the compound at a final DMSO concentration of 2%. 24 h post transfection, the compound containing media was removed and cells were lysed for 20 min at room temperature in 25 µL of passive lysis buffer (Promega) per well. 10µL of the lysate were transferred to a 384 well plate (Corning® low volume 384-well white flat bottom polystyrene NBS microplate, prod. no 3824) and FF-Luc signals were measured 10 min after addition of 10 µL Dual-Glo Luciferase Assay Reagent (Promega) and centrifugation at 500 x g for 1 min. Ren-Luc signals were subsequently measured 10 min after addition of 10 µL Dual-Glo Stop & Glo Luciferase Assay Reagent (Promega) and centrifugation at 500 x g for 1 min. Measurements were conducted with a Tecan Spark reader. Ren-Luc signals were corrected by dividing by the square root of the respective FF-Luc signals to compensate for differences in transfection efficiency and cell density, resulting in relative luminescence signals which are shown as % of the DMSO controls.

Viral infection experiments

A549 (ATCC, CCL-185™) and Vero 76 (ATCC, CRL-1587™) cells were maintained in Dulbecco's modified Eagle's medium (DMEM GlutaMAX, Gibco) supplemented with 3% (v:v) fetal calf serum (FCS; Gibco), non-essential amio acids (NEAA, Gibco) and Penicillin-Streptomycin (Gibco) and kept under 5% CO_2 at 37 °C.

For dose–response inhibition experiments of LASV infection, A549 cells were seeded in 96 well plates at 1×10^4 cells/well. The following day, the medium was removed and cells were infected at an MOI 0.1 with LASV Ba366 (GenBank ID: GU830839) [46, 47] in 50 µL cell culture medium. After 1 h at 37°C, 5% CO_2, the virus inoculum was removed and replaced with 100 µL compound containing medium or the solvent control, both containing 0.5% (v:v) DMSO final. Supernatants were harvested 72 h post infection and frozen at −80°C. To assess the viability of cells, an MTS assay (CellTiter 96® Aqueous) according to the manufacturer's protocol was used. For that, immediately after harvesting the virus-containing supernatant, 120 µL/well of

MTS assay reagent (diluted 1:5 in medium) was added to the cells followed by an incubation at 37°C and 5% CO_2 for 1.5 h. The absorption of the reduced substrate and non-specific background were recorded at 490 and 630 ± 9 nm, respectively, in an Infinite 200 PRO plate reader (Tecan). The background-subtracted values were used for data analysis.

Viral titers were determined by immunofocus assay (IFA) [48-50] using 50 µL of thawed, serially diluted cell culture supernatants for the infection of Vero 76 cells in 96-well plates (2×10^4/well). After 1 h, virus-containing supernatants were replaced with 100 µL overlay medium (1% (w:v) methylcellulose in cell culture medium with 10% (v:v) FCS) and cells were incubated at 37°C and 5% CO_2 for 72 hours. Overlay medium was removed and cells were fixed with 4.5% (v:v) formaldehyde in PBS for 30 min at room temperature. After washing with H_2O, cells were permeabilized for 20 min with 100 µL/well PBS containing 0.5% (v:v) Triton X-100, followed by washing with H_2O and a blocking step (3% FCS in PBS over night at 4°C). For antibody-based detection, the LASV NP-specific mouse monoclonal antibody 2B5 (1:5000 diluted in PBS with 1.5% FCS)[51] was applied for 1 h at room temperature, followed by a washing step and incubation with Peroxidase-conjugated AffiniPure Sheep Anti-Mouse IgG (H+L) (Jackson Immuno Research) secondary antibody (1:1000 diluted in PBS with 1.5% FCS) for 1 h at room temperature. After staining with Tetramethylbenzidin (Immonublot TMB substrate, Mikrogen) NP-positive cell foci/well were quantified and focus-forming units per ml (FFU/ml) of cell culture supernatant were calculated. For all infection experiments, titers for three biological replicates per compound and concentration were determined and normalized to the average of the solvent control (set to 100%).

In vitro polymerase assay

To test for primed polymerase activity in the presence of inhibitors, 0.5 µM LASV L protein was incubated with micafungin or 3'dGTP (control) for 15 min on ice before sequential addition of RNA: 2 µM single-stranded viral 3' RNA (3' HO-GCGUGUCACCUAGGAUCCG-OH 5') as a template, 1 µM fluorescently labeled primer (5' DY649P1-ACGC-OH 3'), and if indicated 2 µM of single-stranded viral 5' RNA (5' HO-GCGCACCGGGGAU-OH 3'). Reactions were conducted in 10 mM HEPES (NaOH), pH 7.0, 50 mM NaCl, 2 mM DTT, 0.1% (w:v) CHAPS and 100 nM sulfo-Cyanine3 dimethyl (as an internal loading control for quantification of product bands) on ice for 15 min. The reaction was started by addition of 2 mM $MnCl_2$ and 1 µM NTPs reaching a final reaction volume of 10 µL. After incubation at 30 °C for 1 h the reaction was

stopped by adding an equivalent volume of 98% formamide, 18 mM EDTA, 0.025 mM SDS, and Orange G and heating the samples at 95 °C for 5 min. Products were separated by denaturing Urea-PAGE (gels: 20% polyacrylamide, 8 M urea, 45 mM tris, 45 mM boric acid, 1 mM EDTA; running buffer: 45 mM tris, 45 mM boric acid, 1 mM EDTA). The gels, measuring 160 x 400 x 0.4 mm, were run at a constant power of 70 W and a temperature > 50°C to ensure the separation of single-stranded RNA. Fluorescence signals were detected using an Amersham Typhoon Biomolecular Imager (Cytiva) with excitation at 635 nm and emission detection at 670 ± 30 nm for the products based on the extended primer and an excitation at 532 nm and emission detection at 570 ± 20 nm for the Cy3 reference channel (loading control). Signals were quantified using ImageQuantTL v10.2 (Cytiva). Curves were fitted using Prism (version 10.6) according to an inhibition vs. response model (three parameters). The labelled primer was chemically synthesised with 5'- DY649P1 modification (Biomers) using the same linker chemistry as for the 5' Cy5 modification of the labeled oligos use in the screening (see Supplementary Fig. S12).

Spectral Shift Experiments

Covalent labeling of lysine residues of LASV L was performed using the Protein Labeling Kit RED-NHS 2nd Generation (NanoTemper). In brief, LASV L was prepared at a final concentration of 5 µM in Labeling buffer, included in the kit, supplemented with 500 mM NaCl. A ten-fold molar excess of dye was added to the protein, followed by incubation for 30 min at room temperature in a total volume of 100 µL in the dark. Buffer exchange to 10 mM HEPES(NaOH) pH 7.0, 200 mM NaCl, 0.1% (w:v) CHAPS and removal of excess dye was done using the B-Column of the labeling kit. The protein concentration after labeling was estimated to 1 µM and the degree-of-labeling was not determined.

Micafungin was prepared as 10 mM stock and diluted in anhydrous DMSO, of which 0.4 µl (1 nM – 200 µM final concentration) was transferred by acoustic dispensing (Echo 550R, Labcyte Inc./Beckmann Coulter) to the assay plates (Dianthus 384-well plate Prod. Nr DI-P001A). 20 µL of 20 nM L protein in 10 mM HEPES(NaOH), pH 7.0, 200 mM NaCl, 0.1% (w:v) CHAPS was added, centrifuged shortly (184 x g, 1 min) and Spectral shift measurements were performed using the Dianthus NT23.PicoDuo (NanoTemper) after 30 min incubation at room temperature. Curves were fitted using Prism (version 10.6) according to a one-site binding model for binding.

In silico docking analysis

For the *in silico* investigation of possible binding sites of micafungin on the RNA-dependent RNA polymerase of Lassa virus (L protein), a docking and cofolding strategy was employed. This was performed using AlphaFold3 [28] and AutoDock Vina [29] to identify consensus ligand-binding sites. Importantly, this approach required the modelling of the full-length L protein, as currently available experimentally determined structures lack several domains.

Modelling the full-length Polymerase (Supplementary Fig. S13)

The elongation-state cryo-EM structure (PDB: 7OJN, EMDB: 12956, 2.92 Å resolution) served as the template for initial L protein models (+/− RNA). The missing pendant domain was modelled based on two structures of the pre-initiation state (PDBs: 7OJK and 7OJJ). These structures were trimmed, leaving 200 residue overlap (N- and C- terminus) with the initial model. Five complete models were generated using MODELLER v10.6 [52] and ranked based on DOPE score [53]. The best scoring model was used as a template to ColabFold (v 1.5.5) [54] to better connect the pendant domain to the core of the L protein through their long loop regions. A final energy minimisation step was performed using the AMBER force field [55].

To derive the complete model of the L elongation state in the presence of RNA L, the RNA conformation derived from the original cryo-EM structure was integrated into the complete RNA-free model using MODELLER, before a final round of energy minimisation.

Binding site identification (Supplementary Fig. S13)

Micafungin binding sites on the L protein were identified using the consensus of two distinct methodologies. First, a blind docking approach was applied using Autodock Vina (v 1.2.0) [29]. Briefly, docking with AutoDock Vina [56] was run 500 times and results combined to ensure conformational space exploration. Parameters were: exhaustiveness 10, 20 models, and a maximum energy difference of 3 kcal/mol. The search box contained all protein atoms (128.188, 112.531, 146.374). To eliminate redundancy, conformations with a root-mean-square deviation (RMSD) $\leq$ 2 Å were represented by the pose with the best vina score. Unique conformations were grouped based on the spatial proximity of their centroid and ranked based on both docking score and cluster population. In the second approach AlphaFold3 was applied for the co-folding of the L protein and micafungin. The LASV Bantou 289 sequence (GenBank: MK044799.1) was used as input together with the corresponding SMILEs (PubChem CID: 477468) representation of micafungin. A total of 1000 seeds were generated

using a local installation of AlphaFold3 with default parameters. For comparison with the docking results, generated models were structurally aligned using the *Superimposer* function from Bio.PDB (Biopython) [57] to the reference model used for docking in the first approach. All models having an RMSD $\leq$ 5.0 Å to the reference model were retained. Subsequently, for each micafungin conformation, protein–ligand contacts were identified by determining the interacting amino acid residues within 5 Å. The micafungin conformations were clustered according to similarities in their residue contact patterns. To further consolidate the clustering results and reduce fragmentation into small clusters, a second hierarchical clustering step was performed, in which individual conformations were reassigned to larger clusters based on centroid distances. Finally, the clusters were ranked based on their ipTM (with the highest score being 0.5) [58].

Clusters obtained by AutoDock Vina docking and AlphaFold3 co-folding were subsequently compared and integrated to identify micafungin-binding sites that are in close proximity (joint binding site). For each cluster, the mean centroid was determined. The Euclidean distance between the mean centroids derived from the two methodologies was then calculated. Clusters were defined as a consensus binding site if the distance between their corresponding averaged centroid was < 6 Å. To reduce the consensus analysis, only the top 20 ranked clusters from the AutoDock Vina results were considered.

Precision docking (Supplementary Fig. 13)

To determine a plausible binding pose for the top-ranked binding site for micafungin, a consensus docking strategy [30] was employed to identify possible poses. This was performed by a hybrid approach, utilizing two docking methods, the latest version of ChemEM [59] and AutoDock Vina (with the Vinardo scoring function)[60]. Initially, ChemEM was used to identify potential binding pockets within the region corresponding to the previously detected ligand-binding cluster. Analysis of the pockets revealed a main cavity consistent with the binding site suggested by the preliminary structural analysis. The centroid of this pocket (-35.9, 4.1, 10.9) was therefore used as the center of the search region for subsequent docking. Given the high conformational flexibility of micafungin, which contains 31 rotatable bonds, two complementary docking strategies were explored. In the first approach, docking of the entire ligand was performed. In the second, micafungin was divided into two fragments: (i) the portion composed of the three terminal aromatic groups and (ii) the macrocycle core in order to sample more efficiently the binding region.

The same docking scheme was applied in parallel using AutoDock Vina. To ensure accurate representation of the protonation state of the ligand, Dimorphite-DL [61] was used to determine the protonation state of micafungin at physiological pH (7.4). The resulting protonated form was then used as input in docking simulations with Vina. In the case of docking the complete molecule, the search region was defined using a cubic grid with dimensions equal to 2.9 times the radius of gyration of the molecule [62], maintaining the same center identified during the pocket identification phase with ChemEM2. The parameters used in both approaches are summarized in Supplementary Table S1.

Finally, the binding pose considered most consistent between the two docking approaches was further refined through a post-processing step with ChemEM (version 0.0.3) [59], using a box sized 30, 30, 30, and centered on the same point used in the previous docking simulations.

Structural analysis

To compare between predicted ligand poses and evaluate structural similarity, root mean square deviation (RMSD) values were calculated. To account for possible permutations of the atomic index resulting from ligand symmetry, symmetry-corrected RMSD calculations were performed using the Python package spyrmsd [63]. The analysis pipeline was implemented via an internal Python script that integrates the spyrmsd library. Visualization of structural models was done using Pymol (Schrödinger) and UCSF ChimeraX [64].

Figure captions

Figure 1: Fluorescence polarization (FP) assay. A) Schematic illustration of the FP assay principle. For explanation see results and methods sections. **B)** Illustration of the tracer design. Linker structures are detailed in Supplementary Fig. S12. RNA models generated using Pymol (version 3.1.3). **C)** Apparent binding affinities (K_D) were determined by titrating 5 nM 3'(1-7)-Cy5 (orange) or 10 nM 5'(0-9)-Cy5 (pink) tracer with increasing concentrations of LASV L-StrepII protein. FP signal was measured after 3h incubation at room temperature (RT) in 10 mM HEPES(NaOH), pH 7.0, 200 mM NaCl, and CHAPS (0.1% (w:v)). Curves were fitted using Prism (version 10.6) according to a one-site binding model. Data points are shown as mean ± SD (n=3). **D)** The FP signals of 10 nM of the tracers only were measured at increasing CHAPS concentrations (in %, w:v) in 10 mM HEPES(NaOH), pH 7.0, 200 mM NaCl after 5 min (t0, solid lines) and 90 min (t1, dotted lines) at RT. Curves for the 5'(0-9)-Cy5

tracer are shown in magenta, for the 3’(1-7)Cy5 tracer in orange. A single nucleotide with the same label (pCp-Cy5) was used as a dye control (grey). Data points are shown as mean ± SD (n=3).

Figure 2: Homogeneous time-resolved Förster resonance energy transfer (HTRF) assay. A) The HTRF assay principle is based on FRET-based fluorescence intensity detection, which is only detectable when the Tb donor coupled to the antibody and the Cy5 acceptor coupled to the viral RNA are in close proximity (~10 nm) (left panel). The long fluorescence lifetime of the Tb cryptate (in the scale of ms) allows for measurment after non-specific fluorescence (in the scale of ns) has declined (right panel). **B)** The influence of increasing Cy5-RNA concentrations as FRET acceptor on the HTRF ratio (representing emission intensities of the FRET-based acceptor normalized to the donor emission, ratio intensity at 665 nm/620 nm) was tested. 0.1 ng/µL anti-His mAb-Tb cryptate FRET donor was mixed with increasing amounts of Cy5-RNA FRET acceptor (0-90 nM) in absence (dashed line) or presence of 75 nM LASV L with either a C-terminal His-StrepII tandem tag (L-His, continuous line) or an internal StrepII-Tag (L-StrepII, negative control, dotted line) in 10 mM HEPES(NaOH), pH 7, 200 mM NaCl, 0.1% (w:v) CHAPS) at RT. 5’(0-9)-Cy5 is shown in magenta, 3’(1-7)-Cy5 in orange. Simple linear regression using Prism (10.6) was used to fit the data. Data points are shown as mean ± SD (n=3).

Figure 3: Displacement vs. competition format. Displacement vs. competition of unlabelled 3‘ and 5‘ RNAs with the Cy5-labeled 3‘ and 5‘ RNAs was tested in the HTRF (A) and FP (B) assays. 3'(1-7) and 5'(0-9) RNAs were used as specific controls while a poly-A9 RNA served as a non-specific control. Conditions without L protein were used to determine the background signals (indicated by grey curve (A) or dotted lines (B)). In displacement format, L protein was first incubated with 3’(1-7)-Cy5 (left panels, yellow squares) or 5’(0-9)-Cy5 (right panels, purple squares), respectively, before the unlabeled RNA (competitor) was added. In competition format, 3’(1-7)-Cy5 (left panels, orange circles) or 5’(0-9)-Cy5 (right panels, magenta circles) was first incubated with the unlabeled RNA before additon of L protein. For the HTRF assay (A), 6 nM 3’(1-7)-Cy5 + 13 nM L protein and 25 nM 5’(0-9)-Cy5 + 25 nM L protein, were used, respectively. For the FP assay, 6 nM 3’(1-7)-Cy5 + 13 nM L protein and 10 nM 5’(0-9)-Cy5 + 50 nM L protein were used, respectively. Since the FP signal increased with increasing concenetrations of 5’(0-9) competitor RNA (see Supplementary Fig. S4), the difference between the conditions with and without L protein (∆FP) is plotted in B. Signals for all experiments were

measured after 3h incubation at RT in 10 mM HEPES(NaOH) pH 7.0, 200 mM NaCl and CHAPS (0.1% (w:v)). Curves were fitted using Prism (version 10.6) according to an inhibition vs. response model (three parameters). Data points are shown as mean ± range (n=2).

Figure 4: **Screening of the Fraunhofer Repurposing collection for inhibition of 3' RNA binding by LASV L protein using the FP and HTRF assay.** Dot plot representations of the inhibition calculated for the whole screening data sets of FP (**A**) and HTRF (**B**) assays with screened compounds colored in light grey, identified hits in orange, positive controls in green (tracer only) and negative controls (tracer plus L protein) in red. Both controls contained an additional 0.05 ng/µL mAb α-6HIS Tb in the HTRF assay. **C)** Measured intensities in the P versus the S channel are shown for the FP assay, color coding as in A. **D)** Measured intensities of the donor versus the acceptor emission in the HTRF assay are presented, color coding as in B. **E)** The correlation of the hits selected in the FP and HTRF assays is shown. Shared hits between FP and HTRF screening are highlighted in orange, additional hits from both screens selected for profiling are colored in light yellow. **F)** Key data of both screens are summarized in the table.

Figure 5: Dose-response curves of selected hits from the 3' RNA screening (A) and the 5' RNA screening (B). A) Hit molecules (see labels of panels) of the 3' RNA screening were tested in the FP (orange curve/dots) and HTRF (brown curve/triangles) assays at a concentration range of 14 nM to 30 µM of the respective compound, 6 nM 3'(1-7)-Cy5, 13 nM LASV L and 0.05 ng/µL mAb-Tb in case of HTRF. Signals were detected after 2h. **B)** 5' RNA screening hit molecules (see labels of panels) were tested in the FP (brown curve/dots) and HTRF (magenta curve/triangles, pink curve/squares) assays at concentrations between 2.5 nM and 50 µM of the respective compound. For FP, 10 nM 5'(0-9)-Cy5 and 50 nM LASV L were used and signals were detected after 3h at RT. For the HTRF assay, 25 nM 5'(0-9)-Cy5, 25 nM LASV L and 0.05 ng/µL MAb-Tb were used with signals detected after 3h (magenta curve/triangles) and 16h (pink curve/squares) at RT. All dose-response experiments were carried out in competition format (preincubation of L and small molecules for 30 min before addition of Cy5-RNAs) in 10 mM HEPES(NaOH), pH 7.0, 200 mM NaCl, and CHAPS (0.1% (w:v)). Compounds were picked from the screening plates. Curves were fitted using Prism (version 10.6) according to an inhibition vs. response model (four parameter, variable slope). Data points are shown as mean ± range (n=2).

Figure 6: Cell-based dose-response experiments. A) The ability of compounds to interfere with viral genome replication and transcription was assessed using the LASV mini-replicon system. Data of two selected compounds, tiplaxtinin and micafungin, are presented. Ribavirin (RBV) was used as a positive control. See methods section for experimental details. Compound concentrations were in the range 22 nM – 100 µM, DMSO concentration was at 2%. Viral genome replication and transcription was quantified via firefly and renilla luciferase signals after cell lysis. Cell viability was determined based on ATP levels using a CellTiter-Glo assay (Promega). Curves were fitted using Prism (version 10.6) according to an inhibition vs. response model (three parameters). Data points are shown as mean ± range of 2 biological replicates (n=2). **B)** The effect of selected compounds (see panel labels) on LASV amplification in A459 cells was assessed. Ribavirin (RBV) and T705 were chosen as controls. Cell were infected in a 96 well format with LASV Ba366 at an MOI of 0.1 for 1h. The virus inoculum was removed and replaced with 100 µL compound containing medium (0.5% DMSO) or the solvent control. Compound concentrations of 20 nM – 33 µM and in a second step also 100 and 200 µM were tested (interrupted curves for transparency). Supernatants containing LASV were harvested 72 h post infection for determination of viral titres by a titration series and an immuno-focus assay (IFA, all samples in technical duplicates). Cell viability was determined using an MTS assay. Data points are shown as the normalized mean of three biological replicates ± SD (n=3).

Figure 7: *In vitro* and *in silico* assessment of the effect of micafungin on L. A) Binding of micafungin to LASV L was demonstrated using spectral shift analysis. For this experiment, 20 nM LASV L, covalently labeled via the lysin residues (RED-NHS 2nd Generation, NanoTemper), was titrated with increasing amounts of micafungin (1 nM – 200 µM) at a final DMSO concentration of 2% in 10 mM HEPES(NaOH), pH 7.0, 200 mM NaCl, and 0.1% (w:v) CHAPS. Spectral shift measurements were performed using the Dianthus NT23.PicoDuo (NanoTemper) after 30 min incubation at RT evaluating a shift of the emission spectra detected at 670 vs. 650 nm. Experiments were performed in three biological replicates (n=3). Curves were fitted using Prism (version 10.6) according to a one-site binding model for binding. K_d and R^2 are provided. **B)** To test for an effect of micafungin on the L protein's RNA polymerase activity, an *in vitro* polymerase assay was performed. 0.5 µM LASV L-StrepII was incubated with different concentrations of micafungin or 3'dGTP as a control (both at a concentration range of 3.3 to 270 µM) for 15 min on ice before sequential addition of RNA as indicated (2 µM 5' RNA, 2 µM 3') and 1

µM of a fluorescently labeled primer in 10 mM HEPES(NaOH), pH 7.0, 50 mM NaCl, 2 mM DTT, 0.1% (w:v) CHAPS and 100 nM sulfo-Cyanine3 dimethyl (as an internal loading control). The reaction was started by the addition of 2 mM $MnCl_2$ and 1 µM NTPs reaching a final reaction volume of 10 µL. After 1 h at 30°C, the RNA products were separated by denaturing Urea-PAGE (20% polyacrylamide, 8M Urea). Fluorescence signals were detected using a Amersham Typhoon Biomolecular Imager (Cytiva). The estimated size of the main product is 21 nt (*). Signals were quantified using ImageQuantTL v10.2 (Cytiva). Curves were fitted using Prism (version 10.6) according to an inhibition vs. response model (three parameters). An uncropped gel image is included in Supplementary Fig. S12. **C)** 2D representation of micafungin, highlighting the three main components we refer to as aromatic tail (green), macrocycle (yellow) and sulphate moiety (red). **D)** Consensus docking results for micafungin in the 5' RNA binding site of the L protein. The consensus clusters (see methods) are shown in purple. For comparison, two close-ups of the 5' RNA binding pocket are presented: (i) containing the micafungin predicted pose and (ii) containing the 5' RNA from the experimentally determined structure (7OJN). The surface around the binding site is semi-transparent with the interacting residues colored in blue for micafungin (i) and violet for the 5' RNA (ii). Micafungin and 5' RNA are presented in black sticks with additional coloring by element. Structures were visualized in ChimeraX.

References

1. Kuhn JH, Adkins S, Alkhovsky SV, An W, Avsic-Zupanc T, Ayllon MA, et al. Annual (2024) taxonomic update of RNA-directed RNA polymerase-encoding negative-sense RNA viruses (realm Riboviria: kingdom Orthornavirae: phylum Negarnaviricota). J Gen Virol. 2025;106(6).
2. Kuhn JH, Brown K, Adkins S, de la Torre JC, Digiaro M, Ergunay K, et al. Promotion of order Bunyavirales to class Bunyaviricetes to accommodate a rapidly increasing number of related polyploviricotine viruses. J Virol. 2024;98(10):e0106924.
3. WHO. Pathogen Prioritization - A scientific framework for epidemic and pandemic research preparedness. https://cdnwhoint/media/docs/default-source/consultation-rdb/prioritization-pathogens-v6finalpdf. 2024.

4. Marien J, Nuismer SL, Magassouba N, Soropogui B, Gunther S, Becker-Ziaja B, et al. Serosurveillance Identifies an Endemic Hotspot of Lassa Fever in Faranah, Upper Guinea. J Infect Dis. 2025;232(5):e830-e8.
5. Moore SM, Rapheal E, Mendoza Guerrero S, Dean NE, Stoddard ST. Estimation of Lassa fever incidence rates in West Africa: Development of a modeling framework to inform vaccine trial design. PLoS Negl Trop Dis. 2025;19(7):e0012751.
6. Hughes JP, Rees S, Kalindjian SB, Philpott KL. Principles of early drug discovery. Br J Pharmacol. 2011;162(6):1239-49.
7. Scherf J, Vogel D, Gul S, Reinshagen J, Gribbon P, Rosenthal M. Limited high-throughput screening compatibility of the phenuivirus cap-binding domain. Sci Rep. 2023;13(1):22820.
8. Lan X, Zhang Y, Jia X, Dong S, Liu Y, Zhang M, et al. Screening and identification of Lassa virus endonuclease-targeting inhibitors from a fragment-based drug discovery library. Antiviral Res. 2022;197:105230.
9. Toba S, Sato A, Kawai M, Taoda Y, Unoh Y, Kusakabe S, et al. Identification of cap-dependent endonuclease inhibitors with broad-spectrum activity against bunyaviruses. Proc Natl Acad Sci U S A. 2022;119(36):e2206104119.
10. Kouba T, Vogel D, Thorkelsson SR, Quemin ERJ, Williams HM, Milewski M, et al. Conformational changes in Lassa virus L protein associated with promoter binding and RNA synthesis activity. Nat Commun. 2021;12(1):7018.
11. Vogel D, Rosenthal M, Gogrefe N, Reindl S, Gunther S. Biochemical characterization of the Lassa virus L protein. J Biol Chem. 2019;294(20):8088-100.
12. Kranzusch PJ, Schenk AD, Rahmeh AA, Radoshitzky SR, Bavari S, Walz T, et al. Assembly of a functional Machupo virus polymerase complex. Proc Natl Acad Sci U S A. 2010;107(46):20069-74.
13. Kranzusch PJ, Whelan SP. Arenavirus Z protein controls viral RNA synthesis by locking a polymerase-promoter complex. Proc Natl Acad Sci U S A. 2011;108(49):19743-8.
14. Peng R, Xu X, Jing J, Wang M, Peng Q, Liu S, et al. Structural insight into arenavirus replication machinery. Nature. 2020;579(7800):615-9.
15. Pyle JD, Whelan SPJ. RNA ligands activate the Machupo virus polymerase and guide promoter usage. Proc Natl Acad Sci U S A. 2019;116(21):10518-24.
16. Xu X, Peng R, Peng Q, Wang M, Xu Y, Liu S, et al. Cryo-EM structures of Lassa and Machupo virus polymerases complexed with cognate regulatory Z proteins identify targets for antivirals. Nat Microbiol. 2021;6(7):921-31.
17. Hall MD, Yasgar A, Peryea T, Braisted JC, Jadhav A, Simeonov A, et al. Fluorescence polarization assays in high-throughput screening and drug discovery: a review. Methods Appl Fluoresc. 2016;4(2):022001.
18. Blay V, Tolani B, Ho SP, Arkin MR. High-Throughput Screening: today's biochemical and cell-based approaches. Drug Discov Today. 2020;25(10):1807-21.
19. Simeonov A, Jadhav A, Thomas CJ, Wang Y, Huang R, Southall NT, et al. Fluorescence spectroscopic profiling of compound libraries. J Med Chem. 2008;51(8):2363-71.
20. Draper DE. A guide to ions and RNA structure. RNA. 2004;10(3):335-43.
21. Silman I, Shnyrov VL, Ashani Y, Roth E, Nicolas A, Sussman JL, et al. Torpedo californica acetylcholinesterase is stabilized by binding of a divalent metal ion to a novel and versatile 4D motif. Protein Sci. 2021;30(5):966-81.

22. Tannous E, Yokoyama K, You DJ, Koga Y, Kanaya S. A dual role of divalent metal ions in catalysis and folding of RNase H1 from extreme halophilic archaeon Halobacterium sp. NRC-1. FEBS Open Bio. 2012;2:345-52.
23. Wallat GD, Huang Q, Wang W, Dong H, Ly H, Liang Y, et al. High-resolution structure of the N-terminal endonuclease domain of the Lassa virus L polymerase in complex with magnesium ions. PLoS One. 2014;9(2):e87577.
24. Malet H, Williams HM, Cusack S, Rosenthal M. The mechanism of genome replication and transcription in bunyaviruses. PLoS Pathog. 2023;19(1):e1011060.
25. Kuzikov M, Reinshagen J, Wycisk K, Corona A, Esposito F, Malune P, et al. Drug repurposing screen to identify inhibitors of the RNA polymerase (nsp12) and helicase (nsp13) from SARS-CoV-2 replication and transcription complex. Virus Res. 2024;343:199356.
26. Reinshagen J, Seashore-Ludlow B, Gadiya Y, Gustavsson AL, Tanoli Z, Aittokallio T, et al. From library to landscape: integrative annotation workflows for compound libraries in drug repurposing. Database (Oxford). 2025;2025.
27. Hass M, Golnitz U, Muller S, Becker-Ziaja B, Gunther S. Replicon system for Lassa virus. J Virol. 2004;78(24):13793-803.
28. Abramson J, Adler J, Dunger J, Evans R, Green T, Pritzel A, et al. Accurate structure prediction of biomolecular interactions with AlphaFold 3. Nature. 2024;630(8016):493-500.
29. Eberhardt J, Santos-Martins D, Tillack AF, Forli S. AutoDock Vina 1.2.0: New Docking Methods, Expanded Force Field, and Python Bindings. J Chem Inf Model. 2021;61(8):3891-8.
30. Houston DR, Walkinshaw MD. Consensus docking: improving the reliability of docking in a virtual screening context. J Chem Inf Model. 2013;53(2):384-90.
31. Gandhi RT, Landovitz RJ, Sax PE, Smith DM, Springer SA, Gunthard HF, et al. Antiretroviral Drugs for Treatment and Prevention of HIV in Adults: 2024 Recommendations of the International Antiviral Society-USA Panel. JAMA. 2025;333(7):609-28.
32. Di Marco L, Cannova S, Ferrigno E, Landro G, Nonni R, Mantia C, et al. A Comprehensive Review of Antiviral Therapy for Hepatitis C: The Long Journey from Interferon to Pan-Genotypic Direct-Acting Antivirals (DAAs). Viruses. 2025;17(2).
33. Sanjuan R, Nebot MR, Chirico N, Mansky LM, Belshaw R. Viral mutation rates. J Virol. 2010;84(19):9733-48.
34. Duffy S. Why are RNA virus mutation rates so damn high? PLoS Biol. 2018;16(8):e3000003.
35. Kulkarni VS, Alagarsamy V, Solomon VR, Jose PA, Murugesan S. Drug Repurposing: An Effective Tool in Modern Drug Discovery. Russ J Bioorg Chem. 2023;49(2):157-66.
36. Wasmann RE, Muilwijk EW, Burger DM, Verweij PE, Knibbe CA, Bruggemann RJ. Clinical Pharmacokinetics and Pharmacodynamics of Micafungin. Clin Pharmacokinet. 2018;57(3):267-86.
37. Farowski F, Cornely OA, Vehreschild JJ, Bauer T, Hartmann P, Steinbach A, et al. Intracellular concentrations of micafungin in different cellular compartments of the peripheral blood. Int J Antimicrob Agents. 2012;39(3):228-31.
38. Okabe A, Carney DW, Tawada M, Akther T, Aida J, Takagi T, et al. Discovery of Highly Potent Noncovalent Inhibitors of SARS-CoV-2 Main Protease through Computer-Aided Drug Design. J Med Chem. 2025;68(20):21330-45.

39. Wang P, Heber D, Henning SM. Quercetin increased bioavailability and decreased methylation of green tea polyphenols in vitro and in vivo. Food Funct. 2012;3(6):635-42.
40. Foster KA, Oster CG, Mayer MM, Avery ML, Audus KL. Characterization of the A549 cell line as a type II pulmonary epithelial cell model for drug metabolism. Exp Cell Res. 1998;243(2):359-66.
41. Boras B, Jones RM, Anson BJ, Arenson D, Aschenbrenner L, Bakowski MA, et al. Preclinical characterization of an intravenous coronavirus 3CL protease inhibitor for the potential treatment of COVID19. Nat Commun. 2021;12(1):6055.
42. Girardin F, Manuel O, Marzolini C, Buclin T. Evaluating the risk of drug-drug interactions with pharmacokinetic boosters: the case of ritonavir-enhanced nirmatrelvir to prevent severe COVID-19. Clin Microbiol Infect. 2022;28(8):1044-6.
43. Childs-Disney JL, Yang X, Gibaut QMR, Tong Y, Batey RT, Disney MD. Targeting RNA structures with small molecules. Nat Rev Drug Discov. 2022;21(10):736-62.
44. Zhang JH, Chung TD, Oldenburg KR. A Simple Statistical Parameter for Use in Evaluation and Validation of High Throughput Screening Assays. J Biomol Screen. 1999;4(2):67-73.
45. Buchholz UJ, Finke S, Conzelmann KK. Generation of bovine respiratory syncytial virus (BRSV) from cDNA: BRSV NS2 is not essential for virus replication in tissue culture, and the human RSV leader region acts as a functional BRSV genome promoter. J Virol. 1999;73(1):251-9.
46. Olschlager S, Lelke M, Emmerich P, Panning M, Drosten C, Hass M, et al. Improved detection of Lassa virus by reverse transcription-PCR targeting the 5' region of S RNA. J Clin Microbiol. 2010;48(6):2009-13.
47. Lecompte E, Fichet-Calvet E, Daffis S, Koulemou K, Sylla O, Kourouma F, et al. Mastomys natalensis and Lassa fever, West Africa. Emerg Infect Dis. 2006;12(12):1971-4.
48. Gunther S, Asper M, Roser C, Luna LK, Drosten C, Becker-Ziaja B, et al. Application of real-time PCR for testing antiviral compounds against Lassa virus, SARS coronavirus and Ebola virus in vitro. Antiviral Res. 2004;63(3):209-15.
49. Asper M, Sternsdorf T, Hass M, Drosten C, Rhode A, Schmitz H, et al. Inhibition of different Lassa virus strains by alpha and gamma interferons and comparison with a less pathogenic arenavirus. J Virol. 2004;78(6):3162-9.
50. Rieger T, Merkler D, Gunther S. Infection of type I interferon receptor-deficient mice with various old world arenaviruses: a model for studying virulence and host species barriers. PLoS One. 2013;8(8):e72290.
51. Hufert FT, Ludke W, Schmitz H. Epitope mapping of the Lassa virus nucleoprotein using monoclonal anti-nucleocapsid antibodies. Arch Virol. 1989;106(3-4):201-12.
52. Sali A, Blundell TL. Comparative protein modelling by satisfaction of spatial restraints. J Mol Biol. 1993;234(3):779-815.
53. Shen MY, Sali A. Statistical potential for assessment and prediction of protein structures. Protein Sci. 2006;15(11):2507-24.
54. Mirdita M, Schutze K, Moriwaki Y, Heo L, Ovchinnikov S, Steinegger M. ColabFold: making protein folding accessible to all. Nat Methods. 2022;19(6):679-82.
55. Maier JA, Martinez C, Kasavajhala K, Wickstrom L, Hauser KE, Simmerling C. ff14SB: Improving the Accuracy of Protein Side Chain and Backbone Parameters from ff99SB. J Chem Theory Comput. 2015;11(8):3696-713.
56. Pena A, Sweeney A, Cook AD, Locke J, Topf M, Moores CA. Structure of Microtubule-Trapped Human Kinesin-5 and Its Mechanism of Inhibition Revealed Using Cryoelectron Microscopy. Structure. 2020;28(4):450-7 e5.

57. Hamelryck T, Manderick B. PDB file parser and structure class implemented in Python. Bioinformatics. 2003;19(17):2308-10.
58. Evans R, O'Neill M, Pritzel A, Antropova N, Senior A, Green T, et al. Protein complex prediction with AlphaFold-Multimer. BioRxiv. 2021.
59. Sweeney A, Mulvaney T, Maiorca M, Topf M. ChemEM: Flexible Docking of Small Molecules in Cryo-EM Structures. J Med Chem. 2024;67(1):199-212.
60. Quiroga R, Villarreal MA. Vinardo: A Scoring Function Based on Autodock Vina Improves Scoring, Docking, and Virtual Screening. PLoS One. 2016;11(5):e0155183.
61. Ropp PJ, Kaminsky JC, Yablonski S, Durrant JD. Dimorphite-DL: an open-source program for enumerating the ionization states of drug-like small molecules. J Cheminform. 2019;11(1):14.
62. Feinstein WP, Brylinski M. Calculating an optimal box size for ligand docking and virtual screening against experimental and predicted binding pockets. J Cheminform. 2015;7:18.
63. Meli R, Biggin PC. spyrmsd: symmetry-corrected RMSD calculations in Python. J Cheminform. 2020;12(1):49.
64. Pettersen EF, Goddard TD, Huang CC, Meng EC, Couch GS, Croll TI, et al. UCSF ChimeraX: Structure visualization for researchers, educators, and developers. Protein Sci. 2021;30(1):70-82.

Acknowledgements

The authors want to thank Ursula Bilitewski, Timm Jessen, Mira Grättinger, Tania Szal, Stephan Günther, and Lisa Oestereich for many helpful discussions throughout the course of this work as well as Elisa Adam for technical support in the BSL-4. We further thank Guendalina Marini for her suggestions with the structural figures. We also acknowledge funding by the German Federal Ministry of Education and research (BMBF), in the meantime renamed to Federal Ministry of Research, Technology and Space (BMFTR) projects 01KI2019 and 01KI2519 to MR. This work has also been funded by the Deutsche Forschungsgemeinschaft (DFG, German Research Foundation) – SFB 1648/1 (2024) – 512741711 and RTG2887 – 497350882. The work in the BSL4 laboratory was supported by the DZIF Infrastructure TTU 01.709.

Figure 1

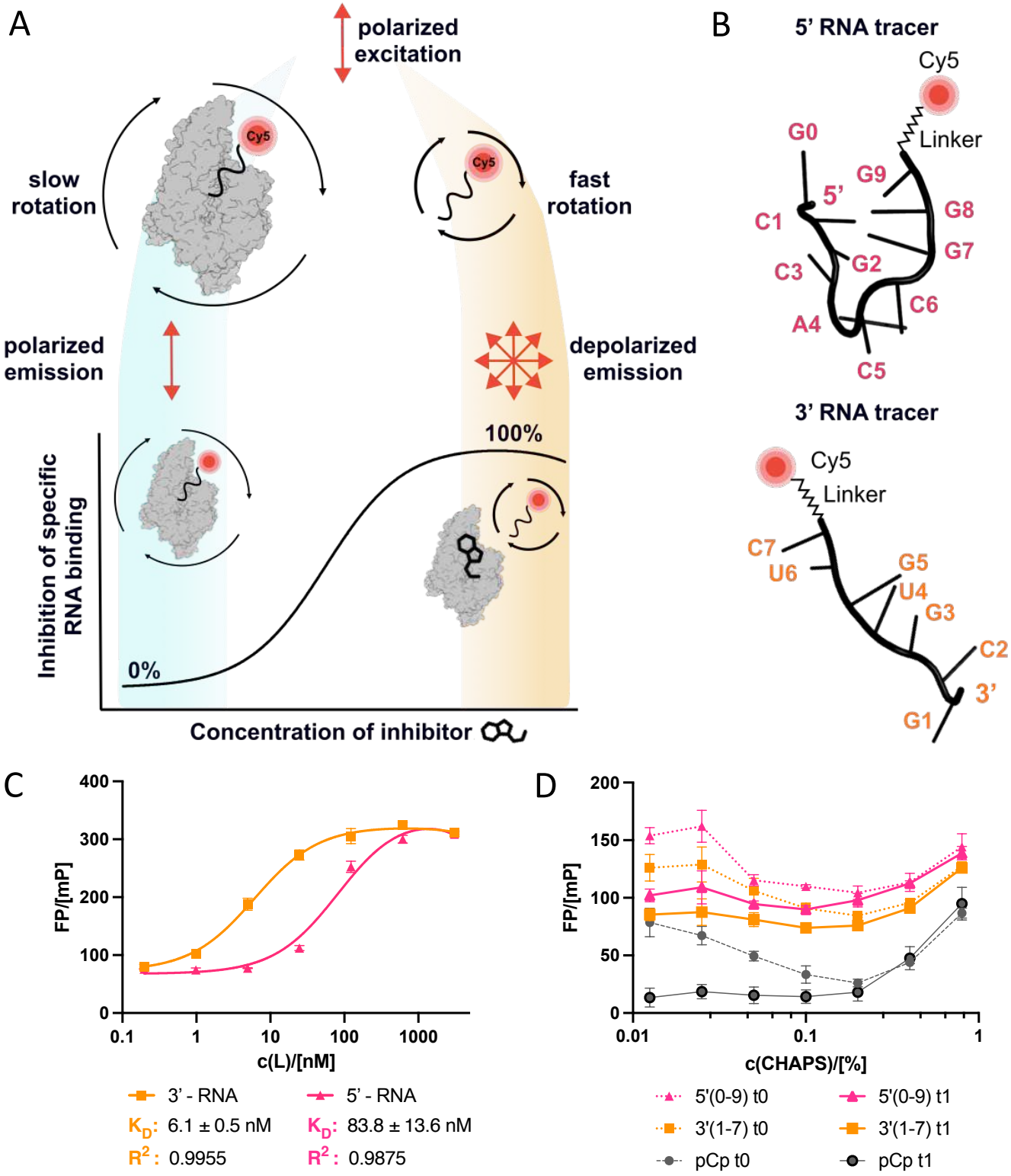


Figure 1: Fluorescence polarization (FP) assay. A) Schematic illustration of the FP assay principle. For explanation see results and methods sections. **B)** Illustration of the tracer design. Linker structures are detailed in Supplementary Fig. S12. RNA models generated using Pymol (version 3.1.3). **C)** Apparent binding affinities (K_D) were determined by titrating 5 nM 3'(1-7)-Cy5 (orange) or 10 nM 5'(0-9)-Cy5 (pink) tracer with increasing concentrations of LASV L-StrepII protein. FP signal was measured after 3h incubation at room temperature (RT) in 10 mM HEPES(NaOH), pH 7.0, 200 mM NaCl, and CHAPS (0.1% (w:v)). Curves were fitted using Prism (version 10.6) according to a one-site binding model. Data points are shown as mean ± SD (n=3). **D)** The FP signals of 10 nM of the tracers only were measured at increasing CHAPS concentrations (in %, w:v) in 10 mM HEPES(NaOH), pH 7.0, 200 mM NaCl after 5 min (t0, solid lines) and 90 min (t1, dotted lines) at RT. Curves for the 5'(0-9)-Cy5 tracer are shown in magenta, for the 3'(1-7)Cy5 tracer in orange. A single nucleotide with the same label (pCp-Cy5) was used as a dye control (grey). Data points are shown as mean ± SD (n=3).

Figure 2

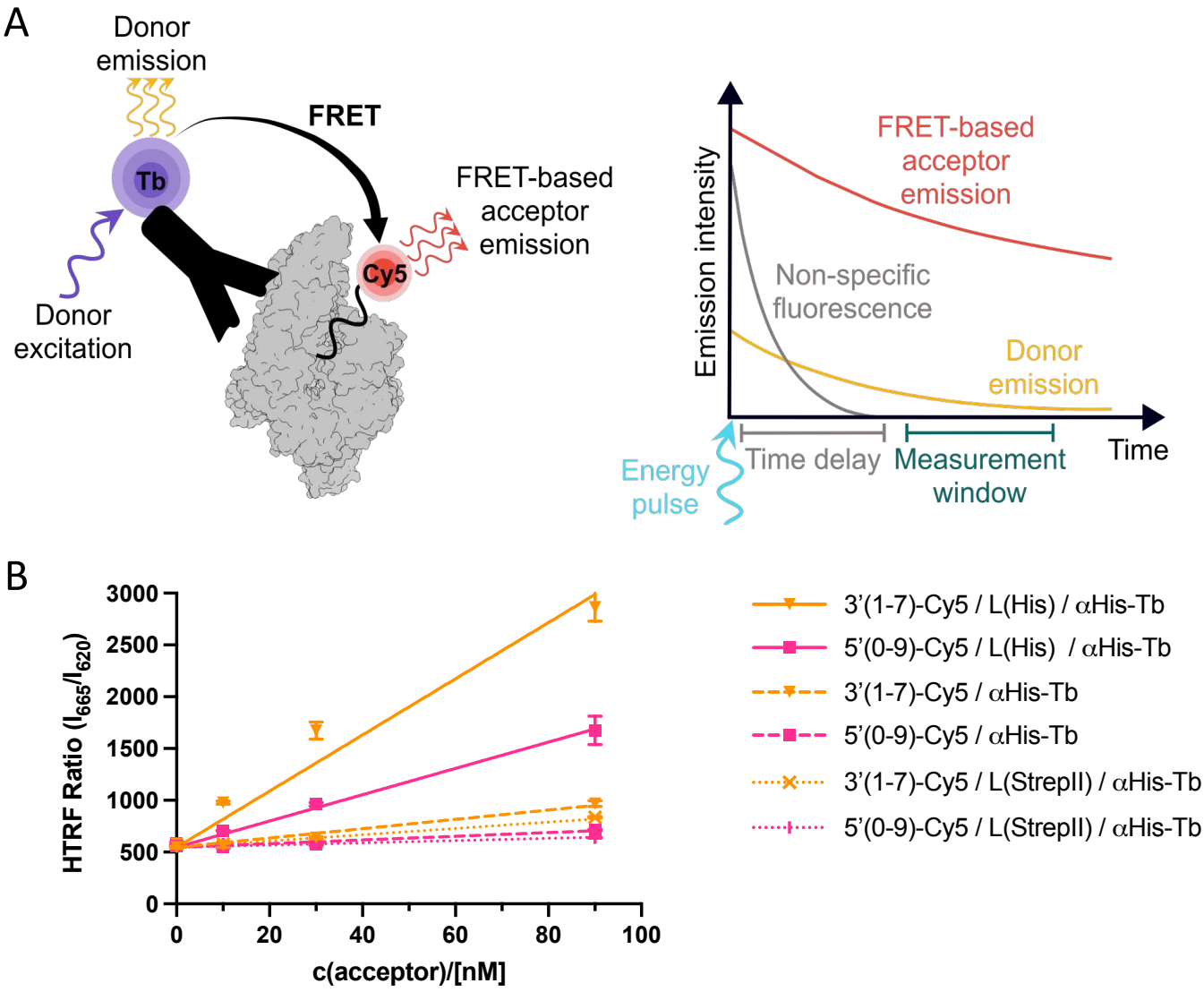


Figure 2: Homogeneous time-resolved Förster resonance energy transfer (HTRF) assay. A) The HTRF assay principle is based on FRET-based fluorescence intensity detection, which is only detectable when the Tb donor coupled to the antibody and the Cy5 acceptor coupled to the viral RNA are in close proximity (~10 nm) (left panel). The long fluorescence lifetime of the Tb cryptate (in the scale of ms) allows for measurment after non-specific fluorescence (in the scale of ns) has declined (right panel). **B)** The influence of increasing Cy5-RNA concentrations as FRET acceptor on the HTRF ratio (representing emission intensities of the FRET-based acceptor normalized to the donor emission, ratio intensity at 665 nm/620 nm) was tested. 0.1 ng/µL anti-His mAb-Tb cryptate FRET donor was mixed with increasing amounts of Cy5-RNA FRET acceptor (0-90 nM) in absence (dashed line) or presence of 75 nM LASV L with either a C-terminal His-StrepII tandem tag (L-His, continuous line) or an internal StrepII-Tag (L-StrepII, negative control, dotted line) in 10 mM HEPES(NaOH), pH 7, 200 mM NaCl, 0.1% (w:v) CHAPS) at RT. 5'(0-9)-Cy5 is shown in magenta, 3'(1-7)-Cy5 in orange. Simple linear regression using Prism (10.6) was used to fit the data. Data points are shown as mean ± SD (n=3).

Figure 3

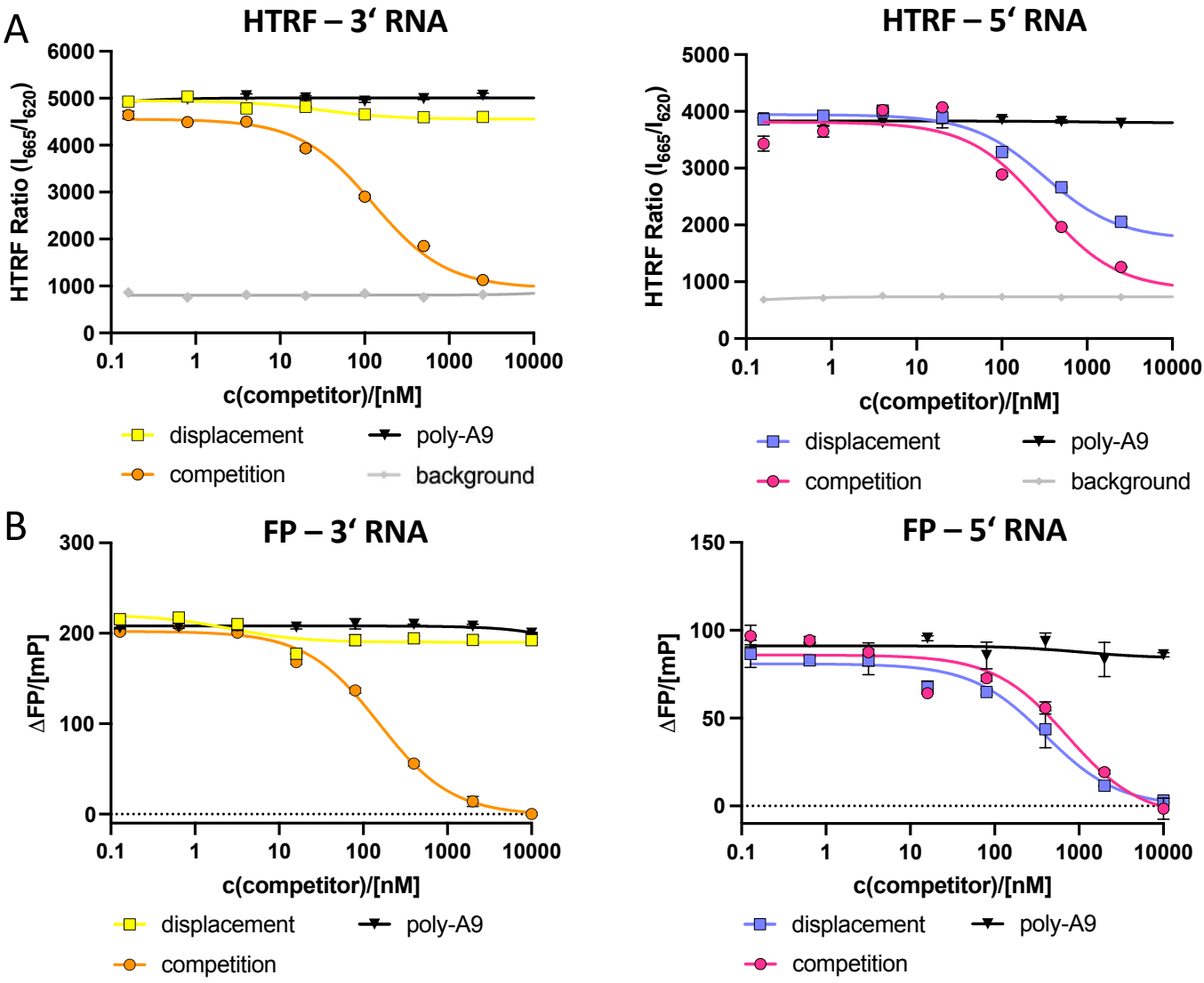
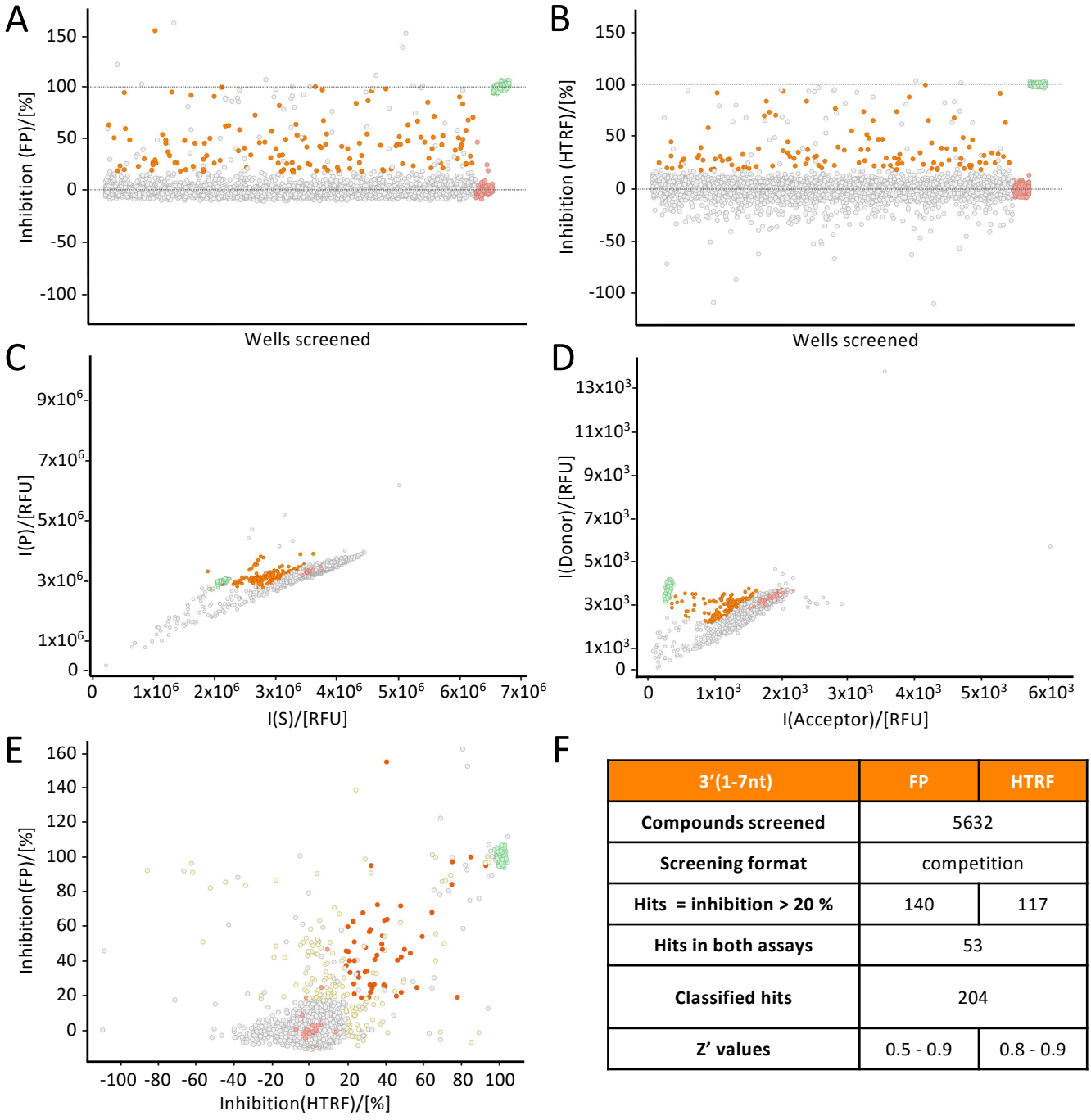


Figure 3: Displacement vs. competition format. Displacement vs. competition of unlabelled 3‘ and 5‘ RNAs with the Cy5-labeled 3‘ and 5‘ RNAs was tested in the HTRF (A) and FP (B) assays. 3'(1-7) and 5'(0-9) RNAs were used as specific controls while a poly-A9 RNA served as a non-specific control. Conditions without L protein were used to determine the background signals (indicated by grey curve (A) or dotted lines (B)). In displacement format, L protein was first incubated with 3’(1-7)-Cy5 (left panels, yellow squares) or 5’(0-9)-Cy5 (right panels, purple squares), respectively, before the unlabeled RNA (competitor) was added. In competition format, 3’(1-7)-Cy5 (left panels, orange circles) or 5’(0-9)-Cy5 (right panels, magenta circles) was first incubated with the unlabeled RNA before additon of L protein. For the HTRF assay (A), 6 nM 3’(1-7)-Cy5 + 13 nM L protein and 25 nM 5’(0-9)-Cy5 + 25 nM L protein, were used, respectively. For the FP assay, 6 nM 3’(1-7)-Cy5 + 13 nM L protein and 10 nM 5’(0-9)-Cy5 + 50 nM L protein were used, respectively. Since the FP signal increased with increasing concenetrations of 5’(0-9) competitor RNA (see Supplementary Fig. S4), the difference between the conditions with and without L protein (ΔFP) is plotted in B. Signals for all experiments were measured after 3h incubation at RT in 10 mM HEPES(NaOH) pH 7.0, 200 mM NaCl and CHAPS (0.1% (w:v)). Curves were fitted using Prism (version 10.6) according to an inhibition vs. response model (three parameters). Data points are shown as mean ± range (n=2).

Figure 4



F

3'(1-7nt)	FP	HTRF
Compounds screened	5632	
Screening format	competition	
Hits = inhibition > 20 %	140	117
Hits in both assays	53	
Classified hits	204	
Z' values	0.5 - 0.9	0.8 - 0.9

Figure 4: **Screening of the Fraunhofer Repurposing collection for inhibition of 3' RNA binding by LASV L protein using the FP and HTRF assay.** Dot plot representations of the inhibition calculated for the whole screening data sets of FP (**A**) and HTRF (**B**) assays with screened compounds colored in light grey, identified hits in orange, positive controls in green (tracer only) and negative controls (tracer plus L protein) in red. Both controls contained an additional 0.05 ng/µL mAb α-6HIS Tb in the HTRF assay. **C)** Measured intensities in the P versus the S channel are shown for the FP assay, color coding as in A. **D)** Measured intensities of the donor versus the acceptor emission in the HTRF assay are presented, color coding as in B. **E)** The correlation of the hits selected in the FP and HTRF assays is shown. Shared hits between FP and HTRF screening are highlighted in orange, additional hits from both screens selected for profiling are colored in light yellow. **F)** Key data of both screens are summarized in the table.

Figure 5

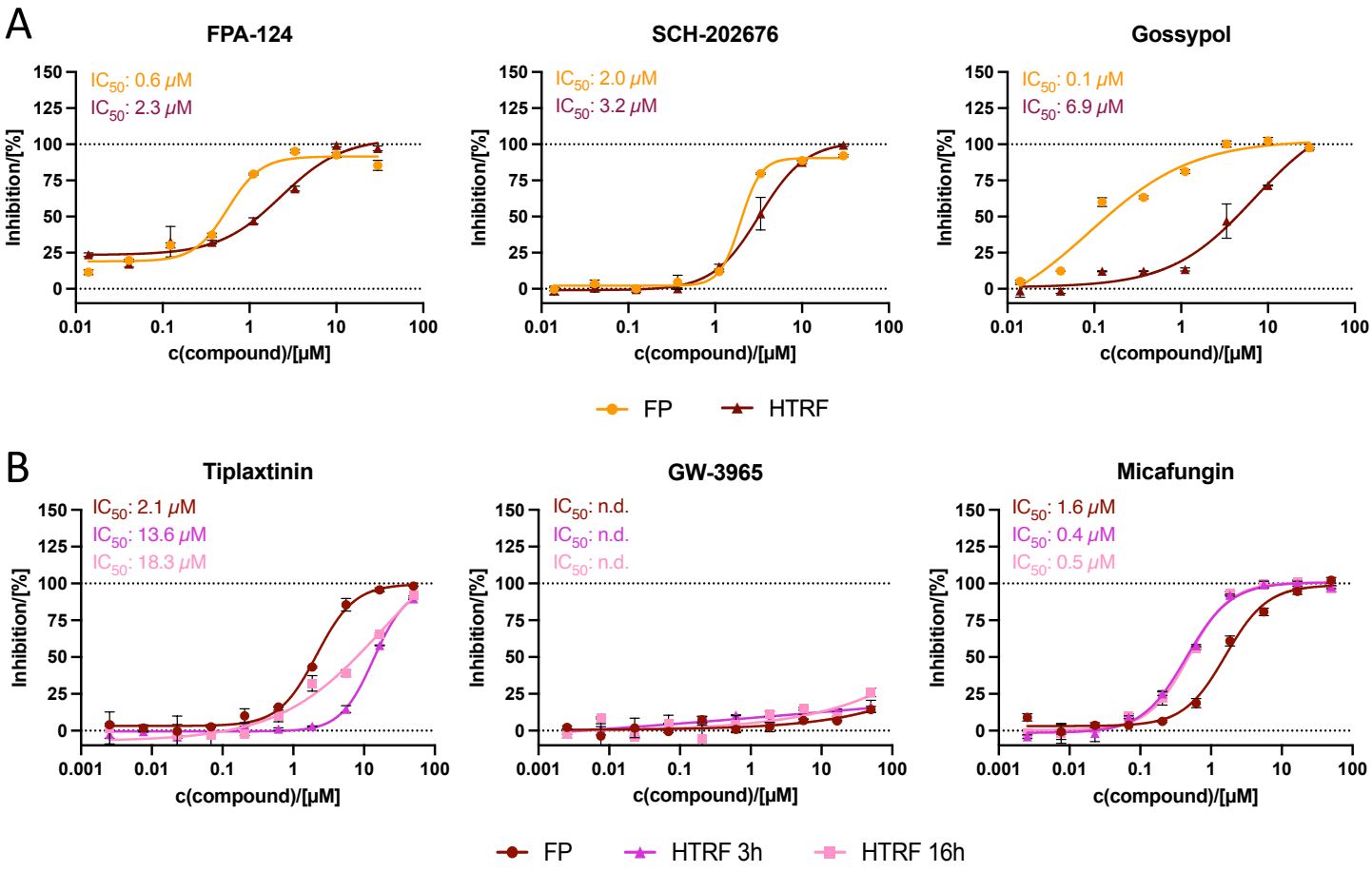


Figure 5: Dose-response curves of selected hits from the 3' RNA screening (A) and the 5' RNA screening (B). A) Hit molecules (see labels of panels) of the 3' RNA screening were tested in the FP (orange curve/dots) and HTRF (brown curve/triangles) assays at a concentration range of 14 nM to 30 µM of the respective compound, 6 nM 3'(1-7)-Cy5, 13 nM LASV L and 0.05 ng/µL mAb-Tb in case of HTRF. Signals were detected after 2h. **B)** 5' RNA screening hit molecules (see labels of panels) were tested in the FP (brown curve/dots) and HTRF (magenta curve/triangles, pink curve/squares) assays at concentrations between 2.5 nM and 50 µM of the respective compound. For FP, 10 nM 5'(0-9)-Cy5 and 50 nM LASV L were used and signals were detected after 3h at RT. For the HTRF assay, 25 nM 5'(0-9)-Cy5, 25 nM LASV L and 0.05 ng/µL MAb-Tb were used with signals detected after 3h (magenta curve/triangles) and 16h (pink curve/squares) at RT. All dose-response experiments were carried out in competition format (preincubation of L and small molecules for 30 min before addition of Cy5-RNAs) in 10 mM HEPES(NaOH), pH 7.0, 200 mM NaCl, and CHAPS (0.1% (w:v)). Compounds were picked from the screening plates. Curves were fitted using Prism (version 10.6) according to an inhibition vs. response model (four parameter, variable slope). Data points are shown as mean ± range (n=2).

Figure 6

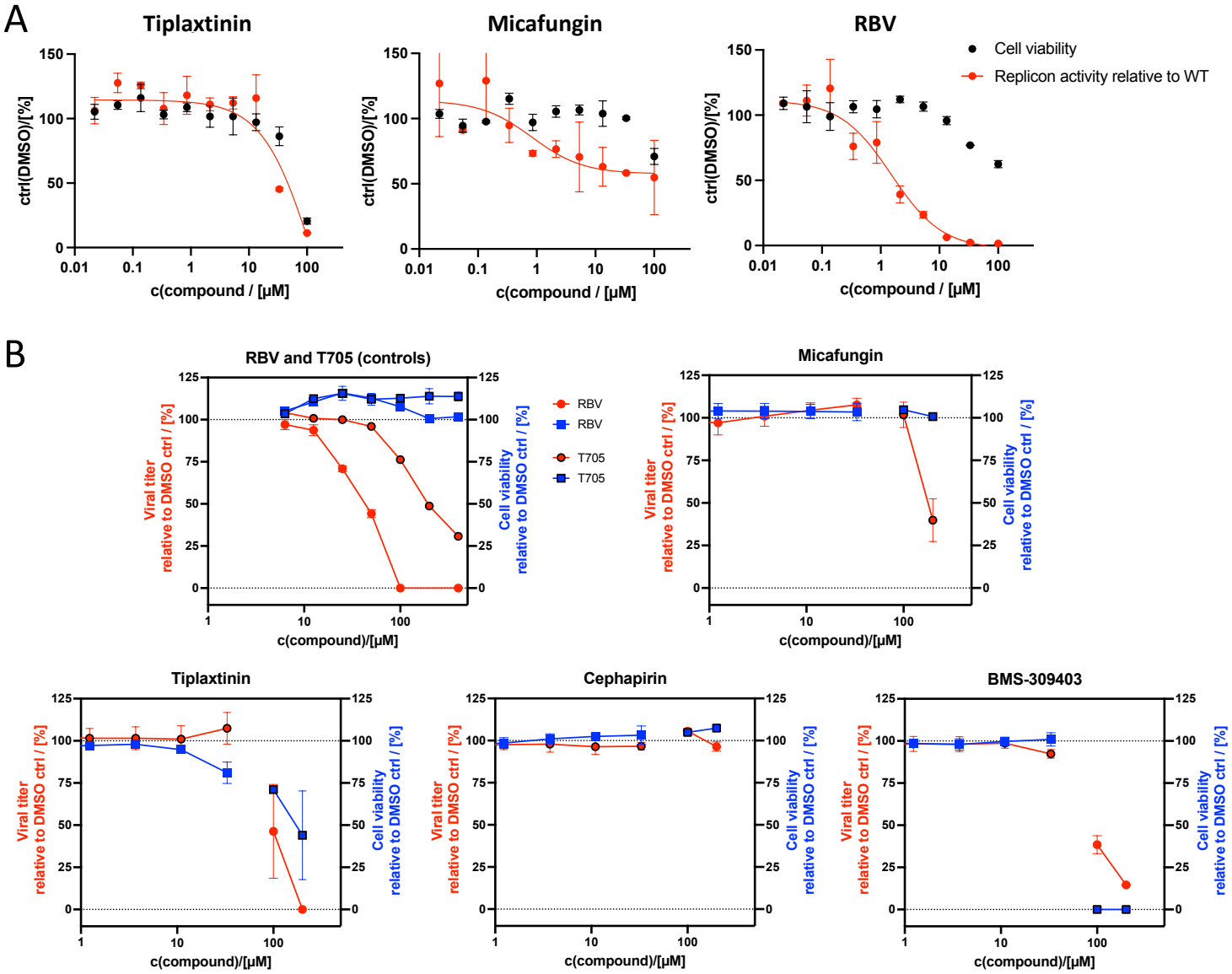
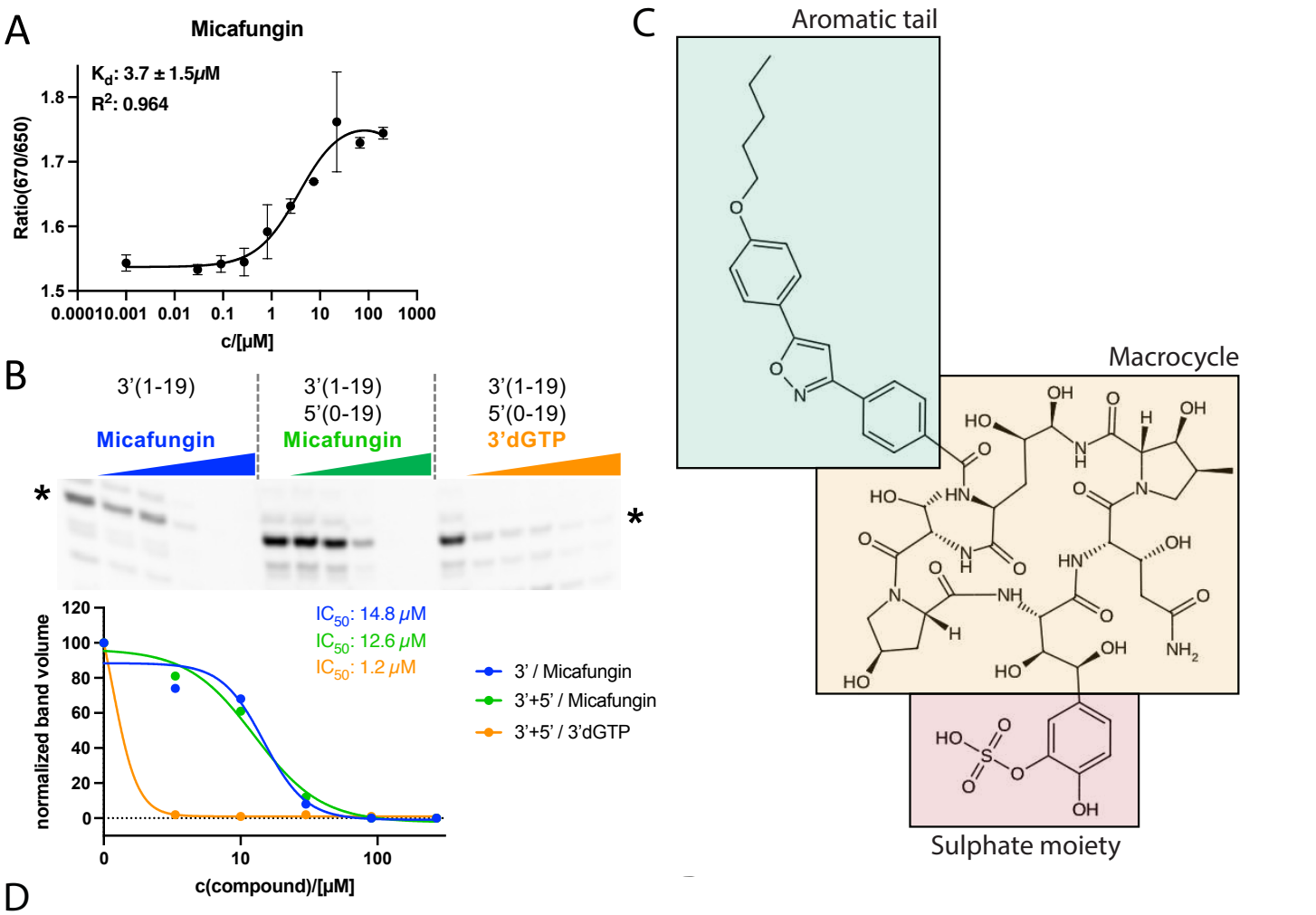


Figure 6: Cell-based dose-response experiments. A) The ability of compounds to interfere with viral genome replication and transcription was assessed using the LASV mini-replicon system. Data of two selected compounds, tiplaxtinin and micafungin, are presented. Ribavirin (RBV) was used as a positive control. See methods section for experimental details. Compound concentrations were in the range 22 nM – 100 µM, DMSO concentration was at 2%. Viral genome replication and transcription was quantified via firefly and renilla luciferase signals after cell lysis. Cell viability was determined based on ATP levels using a CellTiter-Glo assay (Promega). Curves were fitted using Prism (version 10.6) according to an inhibition vs. response model (three parameters). Data points are shown as mean ± range of 2 biological replicates (n=2). **B)** The effect of selected compounds (see panel labels) on LASV amplification in A549 cells was assessed. Ribavirin (RBV) and T705 were chosen as controls. Cell were infected in a 96 well format with LASV Ba366 at an MOI of 0.1 for 1h. The virus inoculum was removed and replaced with 100 µL compound containing medium (0.5% DMSO) or the solvent control. Compound concentrations of 20 nM – 33 µM and in a second step also 100 and 200 µM were tested (interrupted curves for transparency). Supernatants containing LASV were harvested 72 h post infection for determination of viral titres by a titration series and an immuno-focus assay (IFA, all samples in technical duplicates). Cell viability was determined using an MTS assay. Data points are shown as the normalized mean of three biological replicates ± SD (n=3).

Figure 7


A
Micafungin
K_d: 3.7 ± 1.5μM
R^2: 0.964
Ratio(670/650)
c/[μM]
B
3'(1-19)
3'(1-19) 5'(0-19)
3'(1-19) 5'(0-19)
Micafungin
Micafungin
3'dGTP
normalized band volume
IC_{50}: 14.8 μM
IC_{50}: 12.6 μM
IC_{50}: 1.2 μM
3' / Micafungin
3'+5' / Micafungin
3'+5' / 3'dGTP
c(compound)/[μM]
C
Aromatic tail
Macrocycle
Sulphate moiety

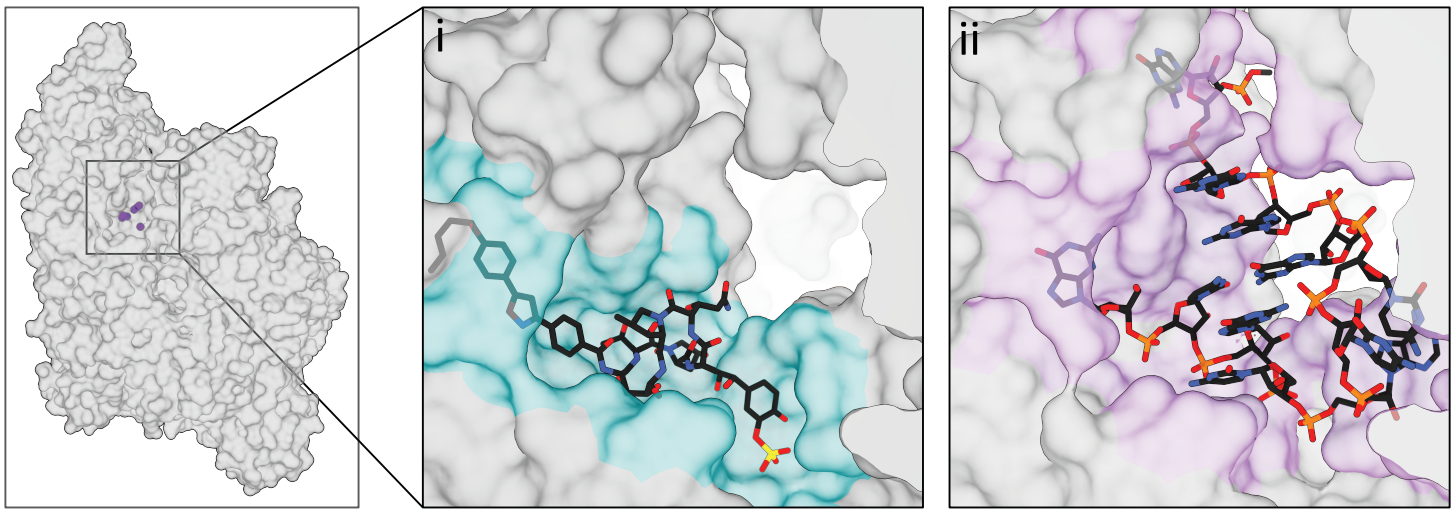

D
i
ii

Figure 7: *In vitro* and *in silico* assessment of the effect of micafungin on L. A) Binding of micafungin to LASV L was demonstrated using spectral shift analysis. For this experiment, 20 nM LASV L, covalently labeled via the lysin residues (RED-NHS 2nd Generation, NanoTemper), was titrated with increasing amounts of micafungin (1 nM – 200 µM) at a final DMSO concentration of 2% in 10 mM HEPES(NaOH), pH 7.0, 200 mM NaCl, and 0.1% (w:v) CHAPS. Spectral shift measurements were performed using the Dianthus NT23.PicoDuo (NanoTemper) after 30 min incubation at RT evaluating a shift of the emission spectra detected at 670 vs. 650 nm. Experiments were performed in three biological replicates (n=3). Curves were fitted using Prism (version 10.6) according to a one-site binding model for binding. K_d and R^2 are provided. **B)** To test for an effect of micafungin on the L protein's RNA polymerase activity, an *in vitro* polymerase assay was performed. 0.5 µM LASV L-StrepII was incubated with different concentrations of micafungin or 3'dGTP as a control (both at a concentration range of 3.3 to 270 µM) for 15 min on ice before sequential addition of RNA as indicated (2 µM 5' RNA, 2 µM 3') and 1 µM of a fluorescently labeled primer in 10 mM HEPES(NaOH), pH 7.0, 50 mM NaCl, 2 mM DTT, 0.1% (w:v) CHAPS and 100 nM sulfo-Cyanine3 dimethyl (as an internal loading control). The reaction was started by the addition of 2 mM $MnCl_2$ and 1 µM NTPs reaching a final reaction volume of 10 µL. After 1 h at 30°C, the RNA products were separated by denaturing Urea-PAGE (20% polyacrylamide, 8M Urea). Fluorescence signals were detected using a Amersham Typhoon Biomolecular Imager (Cytiva). The estimated size of the main product is 21 nt (*). Signals were quantified using ImageQuantTL v10.2 (Cytiva). Curves were fitted using Prism (version 10.6) according to an inhibition vs. response model (three parameters). An uncropped gel image is included in Supplementary Fig. S12. **C)** 2D representation of micafungin, highlighting the three main components we refer to as aromatic tail (green), macrocycle (yellow) and sulphate moiety (red). **D)** Consensus docking results for micafungin in the 5' RNA binding site of the L protein. The consensus clusters (see methods) are shown in purple. For comparison, two close-ups of the 5' RNA binding pocket are presented: (i) containing the micafungin predicted pose and (ii) containing the 5' RNA from the experimentally determined structure (7OJN). The surface around the binding site is semi-transparent with the interacting residues colored in blue for micafungin (i) and violet for the 5' RNA (ii). Micafungin and 5' RNA are presented in black sticks with additonal coloring by element. Structures were visualized in ChimeraX.

3' RNA binding site as target

Compound infos			HTS Inhibition / [%]			In vitro activity IC50 / [µM]				Cell-based activity IC50 / [µM]		Cytotoxicity (MTS)
NAME	PubChem CID	CAS Number	HTRF	FP	FP	HTRF	FP	new batch HTRF	new batch FP	LASV amplification (IFA)	R^2 (IC_{50})	
FPA-124	56972210	902779-59-3	98	97	99	2.3	0.6	1.0	0.1	effect linked to cytotoxicity		high cytotoxicity
SCH-202676	11957689	265980-25-4	98	95	100	3.2	2.0	2.4	1.8	effect linked to cytotoxicity		high cytotoxicity
Gossypol	3503	303-45-7	86	89	99	6.9	0.1	5.8	0.3	effect linked to cytotoxicity		high cytotoxicity
Saroglitazar	60151560	495399-09-2	73	56	75	4.1	16.2	n.d.	n.d	effect linked to cytotoxicity		high cytotoxicity
Thiram	5455	137-26-8	69	68	72	10.0	n.d.	1.0	0.7	effect linked to cytotoxicity		high cytotoxicity
IPA-3	521106	42521-82-4	41	63	80	1.7	1.1	3.6	0.6	effect linked to cytotoxicity		high cytotoxicity
SDZ-220-040	6604839	174575-40-7	38	34	57	10.9	8.0	n.d.	n.d.	not tested		
GW-3965	16078973	405911-17-3	36	95	94	41.7	2.1	n.d.	2.8	effect linked to cytotoxicity		high cytotoxicity
Gambogic Acid	9852185	2752-65-0	35	58	47	n.d.	3.7	n.d.	1.8	effect linked to cytotoxicity		high cytotoxicity
Droxidopa	92974	23651-95-8	35	21	49	8.9	2.3	n.d.	n.d.	not tested		
Salirasib	5469318	162520-00-5	27	45	64	n.d.	3.2	n.d.	3.4	effect linked to cytotoxicity		high cytotoxicity

5' RNA binding site as target

Compound infos			HTS Inhibition / [%]			In vitro activity IC50 / [µM]					Cell-based activity IC50 / [µM]		Cytotoxicity (MTS)
NAME	PubChem CID	CAS Number	HTRF (18h)	FP (n1)	FP (n2)	HTRF (3h)	HTRF (18h)	FP	new batch HTRF	new batch FP	LASV amplification (IFA)	R^2 (IC_{50})	
Tiplaxtinin	6450819	393105-53-8	65	64	73	13.6	18.3	2.1	10.9	5.6	effect linked to cytotoxicity		high cytotoxicity
GW-3965	16078973	405911-17-3	55	108	106	n.d.	n.d.	n.d.	n.d.	1.7	effect linked to cytotoxicity		high cytotoxicity
Micafungin	23666118	208538-73-2	53	77	83	0.4	0.5	1.6	12.2	5.6	195	0.800	none detected
BMS-309403	16122583	300657-03-8	41	60	59	20.2	10.0	5.6	12.4	7.8	effect linked to cytotoxicity		high cytotoxicity
TAK-875	57339446	1374598-80-7	34	47	37	24.4	15.1	13.8	n.d.	n.d.	not tested		
L-755507	9829836	159182-43-1	34	16	31	7.6	7.0	1.2	n.d.	n.d.	not tested		
Salirasib	5469318	162520-00-5	33	33	34	31.2	4.9	2.4	10.9	3.1	effect linked to cytotoxicity		high cytotoxicity
Cefsulodin	656644	52152-93-9	32	27	25	2.6	2.2	4.0	5.3	8.6	no effect		no effect
Cephapirin	23675312	24356-60-3	24	20	26	6.2	5.9	13.2	n.d.	n.d.	no effect		no effect
Avasimibe	166558	166518-60-1	20	52	50	17.8	10.0	8.7	61.4	3.7	not tested		
Saroglitazar	60151560	495399-09-2	19	47	54	19.3	12.0	5.7	n.d.	n.d.	effect linked to cytotoxicity		high cytotoxicity

* data do not represent standard dose-response curves
Blue compounds detected in both 3' and 5' HTS
'n.d.' - non-determinable from the data or not reasonable to determine because of curve fit
'not tested' - experiment not performed

Supplementary Files

This is a list of supplementary files associated with this preprint. Click to download.

- Supplementaryfiles.pdf